

## BACHELOROPPGAVE

BACHELOROPPGAVENS TITTEL	DATO
Target Tracking for Unmanned Surface Vehicles	24.04.2024
	ANTALL SIDER / BILAG
	59 / 17
FORFATTERE	INTERN VEILEDER
Sigurd Aleksander Salomonsen Gresberg, Lars Skogen Johnsen og Sivert Stensrud	Ivar Bjørgo Saksvik

UTFØRT I SAMMARBEID MED	EKSTERN VEILEDER
Oceanlab, OsloMet	

SAMMENDRAG
Dette prosjektet presenterer implementeringen av en modellbasert PID-kontroller for det autonome havfartøyet Otter USV, med mål om å spore et undervannsfartøy slik at Otter er vertikalt over målet. Når Otter er vertikalt over målet vil Otter kunne kommunisere med undervannsfartøyet med et optisk modem som er plassert på Otter. En pole placement algoritme ble brukt for å justere kontrollverdiene og sammenlignet med en empirisk tilnærming. Et simuleringssmiljø ble etablert for testing og validering av kontrollerens ytelse ved bruk av virtuelle mål, etterfulgt av en serie eksperimenter i Oslofjorden. Resultatene viser at Otter USV er i stand til å spore bevegelige mål i rette linjer og sirkler.
Et akustisk lokaliseringssystem og et optisk modem ble i tillegg implementert på fartøyet, for trådløs sporing og kommunikasjon av det undervannsfartøyet. Dette utstyret ble installert ved hjelp av 3D-printede komponenter i nylon for å motstå de store kreftene fra vannforskyvning. På grunn av tidsbegrensninger kunne ikke disse komponentene testes, men ble individuelt verifisert på land.

3 STIKKORD
Target Tracking
Kontrollsystemer
Ubemannet fartøy

# Abstract

This thesis presents the implementation of a model-based PID target-tracking guidance law for the unmanned surface vessel Otter. The objective is to track a submerged underwater vehicle such that the topside vessel is vertically above the target, where coordination between the two vehicles improves the ability for wireless communication between them.

A pole-placement algorithm was used to tune the controller gains and compared to a trial-and-error tuning approach. A simulation environment was established for testing and validation of the controller performance using virtual targets, followed by a series of experiments in the Oslofjord. The experiment results display the Otter USV as able to track moving targets in straight lines and circles.

An acoustic localization system and an optical optical modem was additionally implemented with the vehicle, for the wireless tracking and communication of the submerged target. This equipment was installed by 3D printed mounting brackets in nylon to resist the large drag forces of water displacement. Due to time constraints this equipment was not able to be tested, but was individually verified on land.

# Preface

We would like to thank our supervisor Ivar Bjørge Saksvik for the opportunity to work on this thesis. His availability on short notice, while providing insight and guidance has been invaluable throughout this project.

# Acronyms

**USV** Unmanned Surface Vessel

**GNC** Guidance, Navigation and Control

**INS** Inertial Navigational Systems

**IMU** Inertial Measurement Unit

**GPS** Global Positioning System

**GNSS** Global Navigation Satellite Systems

**RTK** Real-Time Kinematic Positioning

**OBS** On-Board System Control Box

**VCS** Vehicle Control Station

**NED** North-East-Down

**DOF** Degrees of Freedom

**AIS** Automatic Identification System

**PID** proportional-integral-derivative

**SISO** Single-input Single-output

**NMPC** Nonlinear Model Predictive Control

**DRL** Deep Reinforcement Learning

**SBL** Short Baseline

**rpm** Revolutions Per Minute

**FDM** Fused Deposition Modeling

**ASA** Acrylonitrile Styrene Acrylate

**SLS** Selective Laser Sintering

**API** Application Programming Interface

**UOWC** Underwater Optical Wireless Communication

**UGPS** Underwater GPS

# Symbols

$m$	Mass	[kg]
$\psi$	Yaw angle	[rad]
$\tau$	Control force	[N]
$r$	Yaw velocity	[rad/s]
$n_i$	Propeller shaft speed input	[rad/s]
$\omega_b$	Bandwidth frequency	[rad/s]
$\omega_n$	Natural frequency	[rad/s]
$u$	Surge velocity	[m/s]
$x$	Position in x direction	[m]
$y$	Position in y direction	[m]
$z$	Position in z direction	[m]
$d$	Distance to target	[m]
$t_r$	Radius of target	[m]
$K_P$	Controller gain - Proportional	[ $-$ ]
$K_I$	Controller gain - Integral	[ $-$ ]
$K_D$	Controller gain - Derivative	[ $-$ ]

# Contents

<b>1</b>	<b>Introduction</b>	<b>1</b>
1.1	Background . . . . .	1
1.2	Optical Wireless Communication Relay . . . . .	2
1.3	Otter System . . . . .	2
1.4	Literature Review . . . . .	3
1.4.1	Navigation . . . . .	3
1.4.2	Guidance . . . . .	4
1.4.3	Controls . . . . .	4
1.5	Objectives . . . . .	6
1.6	Thesis Outline . . . . .	6
<b>2</b>	<b>Theory</b>	<b>7</b>
2.1	Otter USV Model . . . . .	7
2.1.1	Rigid-Body Matrices . . . . .	8
2.1.2	Added Mass Matrices . . . . .	9
2.1.3	Damping Forces . . . . .	10
2.2	Control Allocation . . . . .	10
2.3	Target Tracking . . . . .	11
2.4	PID Controls . . . . .	12
2.5	Acoustic Underwater Localization . . . . .	14
<b>3</b>	<b>Materials</b>	<b>16</b>
3.1	Otter USV Components . . . . .	16
3.2	Implemented Sensor Systems . . . . .	18
3.2.1	Water Linked Underwater GPS G2 . . . . .	18
3.2.2	Attaching the optical modem . . . . .	20
3.2.3	Mechanical Design for Acoustic Sensor Holder . . . . .	20
3.2.4	Choice of Material & Printing Technology . . . . .	20
3.2.5	Choice of Design . . . . .	21
<b>4</b>	<b>Methods</b>	<b>24</b>
4.1	System Design . . . . .	24
4.2	Application Programming Interface . . . . .	24
4.3	Simulator Development . . . . .	26
4.4	Practical PI and PID Implementation . . . . .	26
4.4.1	Throttle Map . . . . .	26
4.4.2	Practical PI and PID Gain Adjustment . . . . .	29
4.5	Underwater GPS G2 Program Implementation . . . . .	29

4.6	Testing Procedures . . . . .	29
4.6.1	Initial Testing Procedure . . . . .	29
4.6.2	Final Testing Procedure . . . . .	30
<b>5</b>	<b>Results</b>	<b>32</b>
5.1	Initial test results . . . . .	32
5.2	Case 1: Straight Line Target Tracking . . . . .	32
5.2.1	Simulated Results . . . . .	33
5.2.2	Practical Tests . . . . .	33
5.3	Case 2: Circular Target Tracking . . . . .	37
5.3.1	Simulated Results . . . . .	37
5.3.2	Practical Tests . . . . .	38
5.4	Summary of Results . . . . .	42
<b>6</b>	<b>Discussion</b>	<b>43</b>
<b>7</b>	<b>Concluding remarks and further work</b>	<b>46</b>
7.1	Further Work . . . . .	46
<b>A</b>	<b>GitHub Repository</b>	<b>51</b>
<b>B</b>	<b>Software and Hardware</b>	<b>52</b>
<b>C</b>	<b>Otter USV Physical Parameters</b>	<b>53</b>
<b>D</b>	<b>Contribution Table</b>	<b>54</b>
<b>E</b>	<b>Technical drawings</b>	<b>55</b>
<b>F</b>	<b>Gantt Diagram</b>	<b>61</b>
<b>G</b>	<b>Functional Specification</b>	<b>64</b>

# List of Figures

1.1	Otter Unmanned Surface Vessel . . . . .	2
1.2	S-plane illustration with frequency of the damped system $\omega$ , natural frequency $\omega_n$ and damping factor $a$ . . . . .	5
2.1	Otter USV body-frame $\{b\}$ in 6 degrees of freedom. . . . .	7
2.2	Target tracking notation. . . . .	12
2.3	Underwater triangulation ( <i>Illustration by Gresberg, Sigurd A.S., 2024</i> ). . . . .	15
2.4	Concept drawing of acoustic transmitter-receiver relation. . . . .	15
3.1	Otter USV assembled, numbered component list in Table 3.1. . . . .	16
3.2	Assembled Optical Modem and Acoustic Antenna. . . . .	19
3.3	Acoustic transmitter. . . . .	20
3.4	Attachment of the optical sensor. . . . .	20
3.5	Rendered 3D model of the acoustic sensor's clamp and rod support. . . . .	22
3.6	Illustration of carbon fiber layers in the rod support. . . . .	22
3.7	Rendered 3D model of the acoustic sensor's clamp and rod support second iteration. . . . .	23
3.8	Assembled clamp system for the acoustic sensor. . . . .	23
4.1	Otter USV Control system. . . . .	24
4.2	RPM from throttle control signal in left and right thrusters. . . . .	27
4.3	Testing site of initial practical tests, Fillipstadveien 7, 0252 Oslo. . . . .	30
4.4	Testing site of final practical tests, between Gressholmen-Rambergøya and Sjursøya in the Oslofjord. . . . .	31
5.1	Simulated straight line target tracking - Target and vessel path - Pole placement gains . . . . .	33
5.2	Straight line target tracking - Target and vessel path - Pole placement gains . .	34
5.3	Straight line target tracking - Control signals - Pole placement gains . . . . .	34
5.4	Straight line target tracking - Surge and yaw velocity - Pole placement gains . .	35
5.5	Straight line target tracking - Target and vessel path - Trial and error gains . .	36
5.6	Straight line target tracking - Control signals - Trial and error gains . . . . .	36
5.7	Straight line target tracking - Surge and yaw velocity - Trial and error gains . .	37
5.8	Simulated circular target tracking - Target and vessel path - Pole placement gains	38
5.9	Simulated circular target tracking - Target and vessel path - Trial and error gains	38
5.10	Circular target tracking - Target and vessel path - Pole placement gains . . . .	39
5.11	Circular line target tracking - Control signals - Pole placement gains . . . . .	39
5.12	Circular line target tracking - Surge and yaw velocity - Pole placement gains . .	40
5.13	Circular target tracking - Target and vessel path - Trial and error gains . . . .	40
5.14	Circular line target tracking - Control signals - Trial and error gains . . . . .	41



# List of Tables

1.1	Comparison between acoustic and optical communication (Kaushal & Kaddoum, 2016). . . . .	2
2.1	SNAME convention. . . . .	8
2.2	Controller parameters by pole placement . . . . .	14
2.3	Controller parameters by trial & error . . . . .	14
3.1	Otter USV component list. . . . .	17
3.2	Sensors implemented to the Otter USV . . . . .	18
4.1	Otter USV communication methods . . . . .	25
B.1	Software list . . . . .	52
B.2	Hardware list . . . . .	52
C.1	Physical parameters of Otter USV from Maritime Robotics (2020) and Fossen (2023) . . . . .	53

# Chapter 1

## Introduction

### 1.1 Background

With improvements in Guidance, Navigation, and Control (GNC), the use of unmanned surface vessels (USVs) has become relevant for applications such as passenger and freight transport, search and rescue missions, scientific research, and environmental monitoring (Lien Wennersberg, 2023). In May 2023, the autonomous ship Eidsvaag Pioneer traveled 160 nautical miles, displaying functionality in automatic docking, target tracking along the shore and between islands, and collision avoidance with surrounding marine vessels over large distances. A study by Graziano et al. (2016) found that the majority of groundings and collisions in ships were performed on the bridge, where almost a third of accidents included task errors in navigation, and a similar fraction in bridge and task supervision. Traffic monitoring and voyage planning mistakes were also key mistakes, displaying human error as the primary driver of sea collisions. Additionally, Kretschmann et al. (2017) discovered that although the initial cost of autonomous bulk carriers was significantly higher, fuel consumption was estimated to be reduced by 6% and freight rate by 3.4% compared to conventional carriers. Autonomous vessels enhance guidance and control efficiency, thereby reducing the distance traveled and consequently lowering fuel consumption. Where marine craft shipping makes up for more than 90% of the total world trade transport, USVs could produce an environmental, economic, and safety benefit while requiring reduced or no on-board crew (Kim et al., 2015).

USVs have also become an efficient tool in monitoring coastal environments, used to monitor coastal erosion and marine biology, being able to autonomously track and gather data on targets of interest in less accessible areas. Verfuss et al. (2019) and Pocwiardowski (2023) explored systems for monitoring of marine fauna, finding that USVs, which often can stay at sea for months at a time, significantly improve the tracking and monitoring possibilities of marine animals. Compared to autonomous underwater vessels that require dead reckoning or depth measurements to calculate current positions, USVs with continuous satellite signals have a significant advantage in extended deployment, where location can be accurately determined at all times.

In the development of USVs, target tracking and collision avoidance have been core challenges in under- and fully-actuated autonomous vessels. The development of controllers that implement error correction in rudder angles, thruster speeds, and thruster directions are tailored to the specific vessel. This has led to the development guidance laws to minimize positional errors. These strategies utilize control theory, applying to both linear and nonlinear models of the

vessel's kinematics and dynamics.

## 1.2 Optical Wireless Communication Relay

Underwater Optical Wireless Communication (UOWC), while not a new concept, has recently become a greater interest in maritime research (Schirripa Spagnolo et al., 2020). Whereas acoustic communication show promising results in underwater conditions, they are limited by their bandwidth, latency, and data transfer rates. By using visible light in UOWC, a broader bandwidth and higher data rates is achieved, while the ability to send data without interference is much greater, as highlighted in Table 1.1.

	Acoustic	Optical
Range (m)	up to 1000s	$\approx 10 - 100$
Data Rate	kBps	GBps
Speed (m/s)	1500	$2.255 \cdot 10^8$

Table 1.1: Comparison between acoustic and optical communication (Kaushal & Kaddoum, 2016).

Schirripa Spagnolo et al. (2020) also discussed how, while UOWC is limited in its operational range, due to scattering and the light absorption of water molecules, recent research in using lights in the blue-green spectrum could improve on these challenges in transmission distances. By utilizing high-power light-emitting diodes and laser diodes the initial intensity of the optical signal can be increased, improving its travel distance before diminishing.

## 1.3 Otter System



Figure 1.1: Otter Unmanned Surface Vessel.  
Maritime Robotics (2024)

Otter USV, presented in Figure 1.1, is the smallest USV produced by Maritime Robotics, focusing on efficient and precise data acquisition, environmental monitoring, and surveillance. With compact dimensions at 2000x1080x1065 mm and a battery life of up to 20 hours at a velocity of 2 knots, it can easily be deployed in coastal and shallow areas for extended periods of time. The Otter's frame is mounted on two pontoons, with a system control box placed within

the frame, housing most core electronics. With two fixed thrusters, the USV is an underactuated system that utilizes a differential drive in directional changes. The vessel comes with a Vehicle Control Station (VCS), establishing a connection with the Otter, which can be employed to set waypoints in different path-following operations, while providing core information regarding the current state of the vessel. With a small frame and electrical thrusters, the USV can operate quietly without polluting its surroundings.

Two control systems were implemented in the Otter USV, each regulating speed and heading. These are applied in cases of target-tracking in both a simulated environment and real-world target tracking with simulated targets. Additionally, an acoustic receiver and an optical wireless communication relay were attached to the Otter USV in preparation for future submerged target-tracking operations.

## 1.4 Literature Review

GNC systems are considered the most important components of USVs (Liu et al., 2016, pp. 73–75). Through navigation systems, the current and expected state of the USV, that is, its position, velocity, and orientation, is determined through on-board sensors based on the past and current states of the vessel. Guidance systems are responsible for generating desired trajectories through mission and path-planning. The guidance system is cascaded with the navigation and control system to form a feedback loop, which can continuously generate optimal trajectories while ensuring these are physically smooth and feasible, considering the mission goal, environmental conditions, and the capabilities of the USV. The control is responsible for low-level tasks, such as controlling the heading and speed of the vessel. There is also a fourth system known as control allocation for marine vessels, which is responsible for converting the forces and moments from the control system into revolutions per minute (rpm) and rudder angles

### 1.4.1 Navigation

The use of sensing technologies for orientation can be difficult in maritime environments due to the homogeneity of water, generally requiring state estimation to be used for precise positioning (Liu et al., 2016, p. 75). Global Navigation Satellite Systems (GNSS) and Real-time Kinematic (RTK) positioning are regularly used together with Inertial Navigation Systems (INS), enabling continuous tracking of a USVs motion (Stateczny et al., 2021). The INS primarily uses gyroscopes and accelerometers as the main inertial measurement units (IMU), determining the position and velocity through calculations with the angular rates and acceleration. As discussed by Wang et al. (2017, pp. 2–4), errors in the INS accumulated over time can be offset by GNSS, leading to standardization in the use of INS/GNSS integrated systems in maritime navigation. Being able to track moving targets, GNSS is also an important tool in obstacle avoidance. It is used in the Automatic Identification System (AIS) of maritime vessels, which displays nearby maritime vessels, and in tracking significant collision hazards, such as smaller islands or large icebergs. There are currently four commercially available GNSS systems, comprised of BeiDou, Galileo, Glonass, and Navstar Global Positioning System (GPS). Gyroscopes have also had an important role in ship control, with the ability to rotate around any axis, using the principle conservation of angular momentum where it will resist being reorientated by external forces (Fossen, 2021, pp. 313–314). By implementing gyroscopes in the INS, additional information regarding the vessel’s movement and orientation around its axes is obtained.

## 1.4.2 Guidance

In USV guidance systems the tracking schemes are generally divided into categories for target tracking, path following and trajectory tracking (Breivik et al., 2008). Target tracking has the goal of tracking a target where its motion is only known at the moment it occurs. Therefore, no information revolving the future state of the target is available to the system, differing from path following or trajectory tracking, where either the vessel or target movement path is predefined and known to the controllers. Through the vessel state estimation from the navigational systems and sensors to determine the distances to the target, the optimal path to the current target position is determined, requiring a responsive control system with the ability to rapidly adjust heading and velocity based on changes in target positioning. In path following no strict requirements are set, while in trajectory tracking, specific time restrictions are placed, increasing the system complexity as it is required to manage the time to reach each position.

In a simulated target environment, the current state of a target is perfectly determined. However, in real-world applications, sensing technologies are needed, differing by the task requirements. Where LIDAR and radar excel at short-range surface target sensing and obstacle avoidance, in subsea operations it may be more suitable with acoustic, light, and optical sensors (Balestrieri et al., 2021). Like in navigation, the choice and implementation of sensors is crucial in maritime conditions. Difficulties such as large distances without reference points or light absorption and scattering in subsea navigation can limit effectiveness in target tracking.

## 1.4.3 Controls

Control systems consist of interconnected subsystems constructed to achieve the desired system performance in response to specified inputs (Nise, 2011). Their objective is to attain a steady-state response by minimizing the error between the current and the desired states of the system. Additionally, the transient response, which describes how the system reacts when changing from one state to another, is optimized for efficiency.

Control systems utilize readings obtained through the navigation and guidance systems to execute lower-level operational tasks, such as velocity and heading control, in the case of a USV. In systems such as surface vessels and aircraft, the control allocation is also crucial, involving the optimization of actuator usage based on the system's physical limits.

As stated by Fossen (2021), a common optimization method in underactuated USVs involves modeling the vessel as a spring-damped system to implement Lyapunov stability analysis. This analysis aids in designing a control system that is able to accurately calculate the required forces to meet the desired objective, while ensuring system stability. The method is particularly effective in maritime conditions, as it is able to model the dynamic forces acting on the vessel, increasing adaptability to varying states.

### Linear Controllers

The single-input single-output (SISO) linear proportional-integral-derivative (PID) controller is a control loop feedback system widely used in industrial control systems. By deciding a set point, the error between it and the process variable is calculated, adjusting control inputs to minimize the error (Azzeri et al., 2015). These systems are popular due to operational simplicity and low cost, but are generally insufficient in regulating many complex and nonlinear systems. Linear controllers may however prove beneficial in underactuated surface vessels where the

thrusters are fixed, due to the direct relationship between the input signals and the resulting output. Caccia et al. (2008) demonstrated the application of PI and PID controllers to a catamaran-like USV, similar to that of the Otter USV, displaying utility in regulating both heading and speed simply using a compass and GPS in its positioning.

Pole placement is a common method when linearizing nonlinear systems, creating an asymptotically stable system by placing the poles on the left-hand of the s-plane, demonstrated in underwater vessel autopilots as early as Fossen (1991, pp. 98–99). As exhibited in Figure 1.2, by strategically placing the eigenvalues of the system matrix in specific locations, the desired behaviour in velocity, response time, and damping can be achieved.

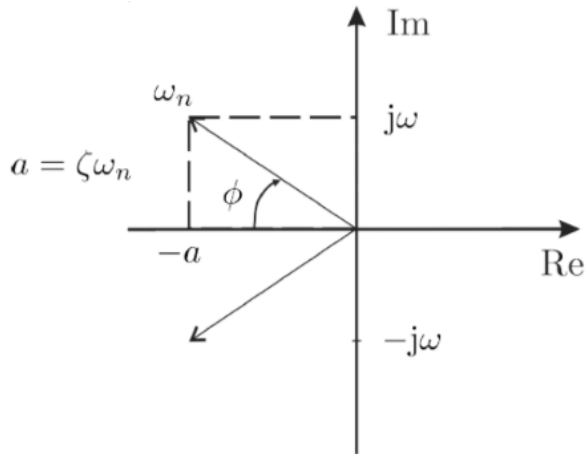


Figure 1.2: S-plane illustration with frequency of the damped system  $\omega$ , natural frequency  $\omega_n$  and damping factor  $a$ .

Fossen (2021, p. 524).

## Nonlinear Controllers

Although the SISO linear PID controller has been widely endorsed in the maritime industry, recent research and practical use have increasingly focused on the implementation of nonlinear controllers as seen in Fossen (2021), Frafjord (2023), and Martinsen et al. (2019). Whereas control methods such as multiple-input multiple-output PID control, Sliding Mode Control, and State Feedback Linearization generally require a linearization of the USV model, Nonlinear Model Predictive Control (NMPC) maintains the model nonlinearity, improving the system's accuracy and future state prediction. The use of NMPC has gained traction in different USV automation problems, displaying functionality in medium-range collision avoidance and target tracking (Akdağ et al., 2022; Frafjord, 2023). A synchronized USV-UAV system developed by Li et al. (2023) with both an autonomous target tracking and landing control highlighted the high accuracy and real-world applications of NMPCs in USVs.

Deep Reinforcement Learning (DRL) has also found increased use in recent years, combining artificial neural networks and reinforcement learning to handle higher-dimensional control problems. By constructing a simulated scenario, the vessel can be trained through thousands of iterations to complete desired tasks. Zhao et al. (2021) presented how employing DRL to several underactuated USVs could improve on the target-tracking problem by developing its model through training in the relevant environments. The DRL USV model was also found to dynamically adjust formation when other USVs fell out of formation, revealing a clear benefit over a linear target tracking model. In a target-interception model by Zhang et al. (2023),

where a USV moves to reach a target attempting to escape while obstructed by obstacles, it found that the DRL model was highly efficient in path prediction of the target given sufficient training. Additionally, it was able to optimize its trajectory around obstructions, ensuring a lower chance of collision or path readjustments when it is met with consequent obstacles shortly afterward.

## 1.5 Objectives

This thesis aims to implement a target-tracking scheme for the Otter USV, owned by OsloMet Oceanlab. The main objectives are as follows:

1. *Using model-based methods such as pole-placement to determine the PID gains and compare these to trial and error gains.*
2. *Determine the optimal performance by modeling of the vessel and practical adjustments of the controller gains.*
3. *Improve on Fossen (2023) Otter USV Simulated environment to more accurately reflect the real-world response by the implementation of surge velocity controls.*
4. *Integrate an acoustic localization system and an optical modem to the Otter USV, and ensure robust mounting brackets for the equipment to handle drag forces from the water as these are submerged.*

The outcome of this project serves as preliminary work in future research on underwater optical communications, requiring the USV to precisely maintain its position vertically above a target. The control systems are engineered to significantly reduce the barrier of entry for conducting future tasks on the Otter USV with any sensor requirement.

## 1.6 Thesis Outline

This thesis is structured into seven chapters, including the introductory chapter, which discusses the background for this thesis. Additionally, relevant literature and the project objectives were presented.

Chapter 2 elaborates on essential theory to understand the kinematic and dynamic forces acting on the vessel, the control allocation, and the methods used to determine the required control parameters. Relevant theory in target tracking through triangulation is also discussed briefly.

Through Chapters 3 and 4 the design, implementation and initial results of the control systems and acoustic sensor attachments in both simulations and real-world tests are elaborated upon. These chapters address design choices, analyzing the need for different implementations.

Finally, Chapters 5, 6, and 7 conclude the thesis, summarizing and reviewing the findings, and discussing future work on the Otter USV.

# Chapter 2

## Theory

Modeling the interplay between the kinematic and dynamic forces acting on the USV is essential in understanding and predicting the vessel's behaviour. This section briefly presents the theory behind the Otter USVs model, control allocation, the applied control laws, and sensor localization methods.

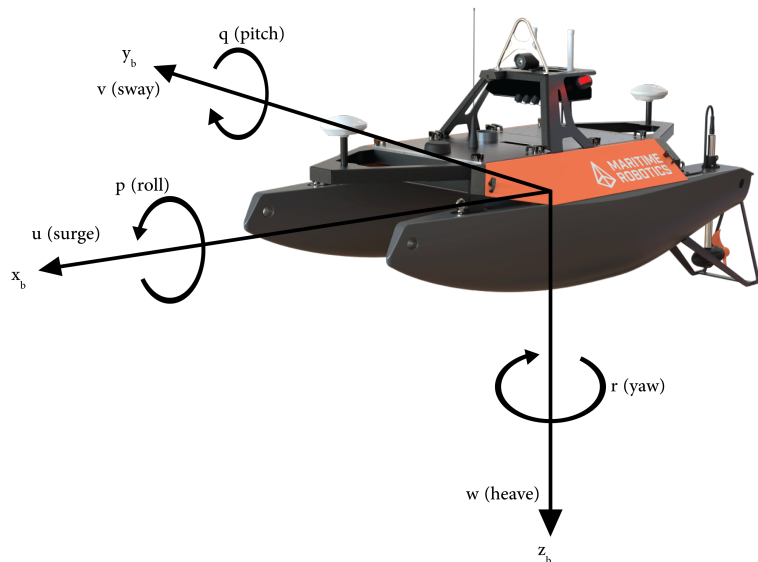


Figure 2.1: Otter USV body-frame  $\{b\}$  in 6 degrees of freedom.

### 2.1 Otter USV Model

The Society of Naval Architects and Marine Engineers (SNAME) notation in Table 2.1 displays the naming conventions used in three degrees of freedom (DOF) for marine vessels (SNAME, 1950).

The equations of motion for a marine craft are given by Fossen's equation:

$$\mathbf{M}\dot{\boldsymbol{\nu}} + \mathbf{C}(\boldsymbol{\nu})\boldsymbol{\nu} + \mathbf{D}(\boldsymbol{\nu})\boldsymbol{\nu} = \boldsymbol{\tau} \quad (2.1)$$

Table 2.1: SNAME convention.

SNAME (1950)					
DOF	Motion	Force & Moment	Linear & Angular Velocity	Position & Euler Angle	
1	Surge	X	u	x	
2	Sway	Y	v	y	
6	Yaw	N	r	$\psi$	

Where  $\mathbf{M}$ ,  $\mathbf{C}(\mathbf{v})$  and  $\mathbf{D}(\mathbf{v})$  respectively denote inertia, Coriolis, and damping matrices of the system, where  $\boldsymbol{\tau}$  are the generalized vector forces or moments acting on the vessel (Fossen, 2021, p. 13). In this case the following assumptions were made:

1. *The wind and wave forces acting on the vessel,  $\boldsymbol{\tau}_{wind}$  and  $\boldsymbol{\tau}_{wave}$ , are neglected.*
2. *The buoyant and gravitational forces,  $\mathbf{g}(\boldsymbol{\eta})$ , and the restoring moments from ballast,  $\mathbf{g}_o$ , are neglected.*
3. *The Otter is modeled in 3 DOF, neglecting Heave, Roll, and Pitch.*

The kinematics  $\boldsymbol{\eta}$ , with the USV position and yaw ( $\psi$ ), as well as the velocity vectors, in the inertial frame  $\{n\}$ , are given by:

$$\boldsymbol{\eta} = [x \ y \ \psi]^T \quad (2.2)$$

$$\dot{\boldsymbol{\eta}} = [\dot{x} \ \dot{y} \ \dot{\psi}]^T \quad (2.3)$$

In the body-frame  $\{b\}$ , the dynamics  $\boldsymbol{\nu}$  with surge, sway, and yaw rate can then be expressed as:

$$\boldsymbol{\nu} = [u \ v \ r]^T \quad (2.4)$$

A transformation between body-frame  $\{b\}$  and the inertial frame  $\{n\}$  in north-east-down (NED) coordinates is done with a rotation matrix,  $\mathbf{R}_b^n(\psi)$ , for 3 DOF (Fossen, 2021, p. 22; Saksvik et al., 2022):

$$\dot{\boldsymbol{\eta}} = \mathbf{R}_b^n(\psi)\boldsymbol{\nu} \quad (2.5)$$

with the transformation matrix:

$$\mathbf{R}_b^n(\psi) = \begin{bmatrix} \cos(\psi) & -\sin(\psi) & 0 \\ \sin(\psi) & \cos(\psi) & 0 \\ 0 & 0 & 1 \end{bmatrix} \in SO(3) \quad (2.6)$$

### 2.1.1 Rigid-Body Matrices

To find the total system inertia  $\mathbf{M}$  and Coriolis  $\mathbf{C}(\boldsymbol{\nu})$  In 3 DOF, the rigid-body kinetics are expressed in matrix-vector form by (Fossen, 2021, p. 55):

$$\mathbf{M}_{RB}\dot{\boldsymbol{\nu}} + \mathbf{C}_{RB}(\boldsymbol{\nu})\boldsymbol{\nu} = \boldsymbol{\tau}_{RB} \quad (2.7)$$

Following the simplified 3 DOF model by Fossen (2021, p. 156), the generalized forces  $\tau_{RB} = [X \ Y \ N]^T$  are expressed in the body-frame  $\{b\}$ , where  $M_{RB}$  and  $C_{RB}(\nu)$  sequentially denote the rigid-body mass matrix, and the rigid-body Coriolis and centripetal matrix due to rotation of the body-frame  $\{b\}$  about the inertial frame  $\{n\}$ :

$$M_{RB} = \begin{bmatrix} m & 0 & 0 \\ 0 & m & mx_g \\ 0 & mx_g & I_z \end{bmatrix} \quad (2.8)$$

$$C_{RB}(\nu) = \begin{bmatrix} 0 & -mr & -mx_gr \\ mr & 0 & 0 \\ mx_gr & 0 & 0 \end{bmatrix} \quad (2.9)$$

where  $m$  is the total mass including payloads,  $x_g$  the center of gravity from the reference point, and  $I_z$  the inertia of the z-axis around the body-frame  $\{b\}$ . The inertia matrix is denoted as:

$$I_g = \begin{bmatrix} I_x & -I_{xy} & -I_{xz} \\ -I_{yx} & I_y & -I_{yz} \\ -I_{zx} & -I_{zy} & I_z \end{bmatrix} = m \begin{bmatrix} R_{44}^2 & 0 & 0 \\ 0 & R_{55}^2 & 0 \\ 0 & 0 & R_{66}^2 \end{bmatrix} \quad (2.10)$$

Respectively,  $R_{44}$ ,  $R_{55}$  and  $R_{66}$  denote the radii of gyration around roll, pitch, and yaw.

### 2.1.2 Added Mass Matrices

The mass and how loads are dispersed in a vessel dictates the inertia added to a system from having to displace fluids surrounding the vessel as they cannot simultaneously inhabit the same space. Added mass leads to reduced acceleration and maneuverability, and influences the natural frequency of the vessel's oscillations (Techet, 2005). Fossen (2021, p. 147) presents the added mass matrix for 3 DOF as:

$$M_A = - \begin{bmatrix} X_{\dot{u}} & 0 & 0 \\ 0 & Y_{\dot{v}} & Y_{\dot{r}} \\ 0 & Y_{\dot{r}} & N_{\dot{r}} \end{bmatrix} \quad (2.11)$$

Where  $X_{\dot{u}}$  represents the total effect of added mass in surge,  $Y_{\dot{v}}$  for sway and  $N_{\dot{r}}$ . Given the multipliers assumed in Fossen (2023), these values are given by:

$$X_{\dot{u}} = -0.1 \cdot m \approx -6.2 \quad (2.12)$$

$$Y_{\dot{v}} = -1.5 \cdot m \approx -93 \quad (2.13)$$

$$N_{\dot{r}} = -1.7 \cdot (m \cdot R_{66}^2 + m \cdot 0.2) \approx -30.57 \quad (2.14)$$

With  $N_{\dot{r}}$  also considering the center of gravity offset of 0.2 meters from the Otter central cross-section. The added mass Coriolis-centripetal matrix  $C_A(\nu)$  for surface vessels is presented in Fossen (2021, p. 147) being:

$$\mathbf{C}_A(\boldsymbol{\nu}) = \begin{bmatrix} 0 & 0 & Y_v v_r + Y_r r \\ 0 & 0 & -X_u u_r \\ -Y_v v_r - Y_r r & X_u u_r & 0 \end{bmatrix} \quad (2.15)$$

Finally the total inertia and Coriolis matrices  $\mathbf{M}$  and  $\mathbf{C}(\boldsymbol{\nu})$  can be determined by the sum of the rigid-body matrices (2.9, 2.8) and the added mass matrices (2.11, 2.15):

$$\mathbf{M} = \mathbf{M}_{RB} + \mathbf{M}_A \quad (2.16)$$

$$\mathbf{C}(\boldsymbol{\nu}) = \mathbf{C}_{RB}(\boldsymbol{\nu}) + \mathbf{C}_A(\boldsymbol{\nu}) \quad (2.17)$$

### 2.1.3 Damping Forces

The linear damping matrix, which quantifies the dissipative forces from fluid resistance and friction in surge, sway, and yaw, is detailed by Fossen (2021, p. 150) as:

$$\mathbf{D} = - \begin{bmatrix} X_u & 0 & Y_r \\ 0 & Y_v & Y_r \\ 0 & N_v & N_r \end{bmatrix} \quad (2.18)$$

While neglecting the damping forces in sway ( $Y_v \approx 0$ ) due to hull symmetry, following Fossen (2023), the remaining dissipative forces are determined by:

$$X_u = \frac{-24.4 \cdot g}{u_{max}} \approx -77.55 \quad (2.19)$$

$$N_r = \frac{-M_{66}}{T_{yaw}} \approx -51.03 \quad (2.20)$$

With a maximum surge velocity of  $u_{max} \approx 3.08$  m/s, and a time constant of one second, with  $X_u$  and  $N_r$  consequently indicating the the linear and angular damping in surge and yaw.

## 2.2 Control Allocation

The control allocation analyzes the effect of control commands to the system's actuators to determine the actuator outputs, improving the efficiency in reaching desired states. This process accurately decides the relationship between input signals to output propeller rpm (Fossen, 2021).

While the wind and wave forces,  $\tau_{wind}$  and  $\tau_{wave}$ , are neglected for more predictable operating conditions, the control forces  $\boldsymbol{\tau}$  can be solved by the equation:

$$\boldsymbol{\tau} = \mathbf{T} \mathbf{K} \mathbf{u} \quad (2.21)$$

with  $\mathbf{T}$  as the thruster configuration matrix and  $\mathbf{K}$  the diagonal matrix of thruster coefficients (Fossen, 2021, pp. 319–321). The control variable  $\mathbf{u}$  is given by:

$$\mathbf{u} = \begin{bmatrix} u_1 \\ u_2 \end{bmatrix} = \begin{bmatrix} n_1 & |n_1| \\ n_2 & |n_2| \end{bmatrix} \quad (2.22)$$

Which solved for  $n_i$  grants the propeller rpm. The thrusters only act on surge and yaw, therefore  $\boldsymbol{\tau}$  in 6 DOF can be denoted as:

$$\boldsymbol{\tau} = [\tau_1 \ 0 \ 0 \ 0 \ 0 \ \tau_6]^T \quad (2.23)$$

Where  $\tau_1$  and  $\tau_6$  respectively detail the control signals for surge and yaw. The matrices for the control forces are expanded by using (2.23) with (2.21):

$$\begin{bmatrix} \tau_1 \\ \tau_6 \end{bmatrix} = \begin{bmatrix} 1 & 1 \\ -l_1 & -l_2 \end{bmatrix} \begin{bmatrix} k_1 & 0 \\ 0 & k_2 \end{bmatrix} \begin{bmatrix} u_1 \\ u_2 \end{bmatrix} \quad (2.24)$$

And by solving for  $\mathbf{u}$ , yielding the equation for the control variable:

$$\begin{bmatrix} u_1 \\ u_2 \end{bmatrix} = \begin{bmatrix} k_1 & 0 \\ 0 & k_2 \end{bmatrix}^{-1} \begin{bmatrix} 1 & 1 \\ -l_1 & -l_2 \end{bmatrix}^{-1} \begin{bmatrix} \tau_1 \\ \tau_6 \end{bmatrix} \quad (2.25)$$

Furthermore, by solving (2.22) for  $n_i$ , the rpm to the given control variable is calculated

$$\begin{bmatrix} n_1 \\ n_2 \end{bmatrix} = \begin{bmatrix} \text{sgn}(u_1)\sqrt{|u_1|} \\ \text{sgn}(u_2)\sqrt{|u_2|} \end{bmatrix} \quad (2.26)$$

$$\text{sgn}(x) = \begin{cases} -1 & \text{if } x < 0 \\ 0 & \text{if } x = 0 \\ 1 & \text{if } x > 0 \end{cases} \quad (2.27)$$

## 2.3 Target Tracking

Drawing from the target tracking scheme established in Wan et al. (2019), as seen in Figure 2.2, given the vessel kinematics for 3 DOF in equation 2.2, the total distance from the vessel to the desired target distances  $x_t$  and  $y_t$  is determined by:

$$d = \sqrt{(x - x_t)^2 + (y - y_t)^2} \quad (2.28)$$

Granted the notation visualized in Figure 2.2 (Wan et al., 2019), the current errors along the x- and y-axis in the inertial frame  $\{n\}$ ,  $x_e$  and  $y_e$ , are acquired from

$$x_e = (x - x_t) \cdot \cos(\psi) \quad (2.29)$$

$$y_e = (y - y_t) \cdot \sin(\psi) \quad (2.30)$$

Similarly, the desired heading angle is gauged

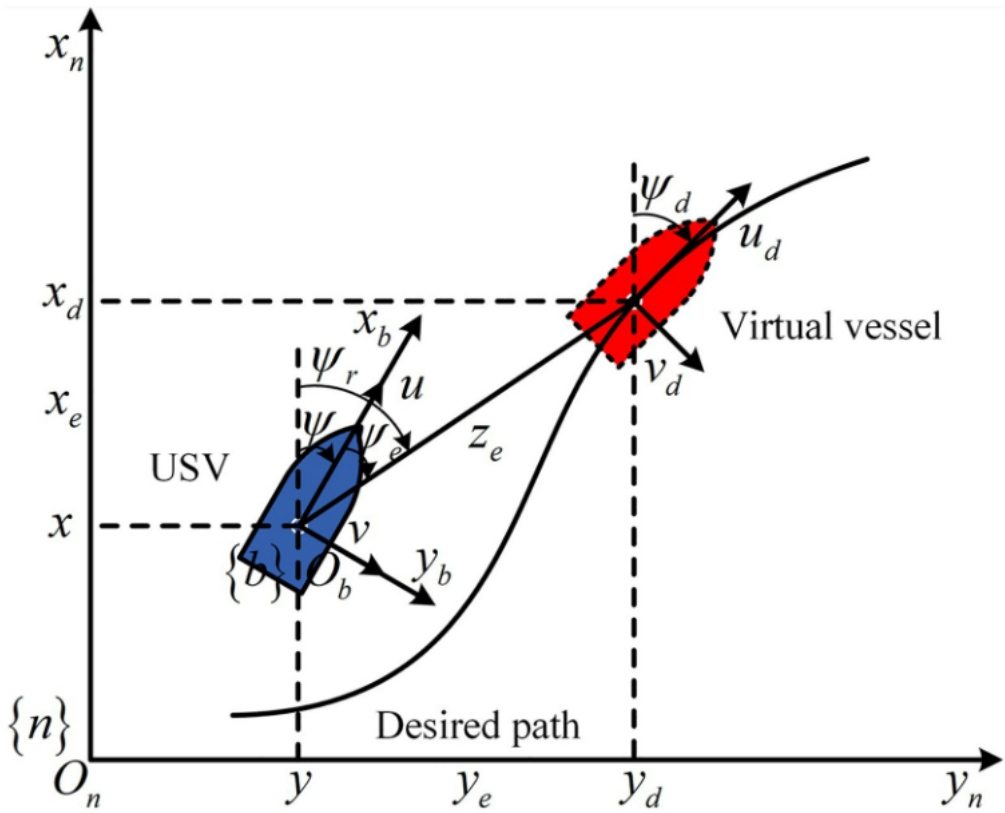


Figure 2.2: Target tracking notation.  
Wan et al. (2019).

$$\psi_d = \text{mod}(\alpha + \pi, 2\pi) - \pi \quad (2.31)$$

The modulo operation is computed to ensure the angle to target  $\psi_d$  returns to no larger or smaller than the  $[-\pi, \pi]$  range, where  $\alpha$  is the difference between current heading  $\psi$  and the tangential angle between the x-axis and the target  $\psi_p$ :

$$\psi_p = \text{atan2}(x_e, y_e) \quad (2.32)$$

## 2.4 PID Controls

When neglecting vertical movement, the USV is modeled as a pure linear mass-damper system (Fossen, 2021, pp. 523–524) and can be modeled as:

$$m\ddot{x} + d\dot{x} + kx = \tau, \quad k = 0 \quad (2.33)$$

The controls are split into two SISO linear PID controllers due to the Otter system underactuation, separately controlling the surge and heading. From 2.28 and 2.31 the surge and heading control error is found by:

$$\tilde{x} = d - t_r \quad (2.34)$$

$$\tilde{\psi} = \psi_d - \psi \quad (2.35)$$

Where  $\tilde{x}$  signifies the error in surge from the radii where the target is considered in range ( $t_r$ ) minus the distance from target, and similarly  $\tilde{\psi}$ , the error in desired yaw. Based on traditional PID control (Ang et al., 2005), the control law scheme for both controllers in surge and heading, with the control errors in equation 2.34 and 2.35, are then given by:

$$\tau_1 = K_{p,x}\tilde{x} + K_{d,x}\dot{\tilde{x}} + K_{i,x} \int_0^t \tilde{x} dt \quad (2.36)$$

$$\tau_6 = K_{p,\psi}\tilde{\psi} + K_{d,\psi}\dot{\tilde{\psi}} + K_{i,\psi} \int_0^t \tilde{\psi} dt \quad (2.37)$$

## Pole Placement

According to Fossen (2021), in a typical mass-damper-spring system for marine crafts, the damping ratio should be close to a critically damped system  $\zeta = 1$  to ensure rapid response times without overshooting setpoints. As described in Fossen (2021, pp. 523–529), the pole placement tuning rules in a SISO linear PID controller when  $k = 0$  are then given by:

$$\omega_n = \frac{1}{\sqrt{1 - 2\xi^2 + \sqrt{4\xi^4 - 4\xi^2 + 2}}} \omega_b \quad (2.38)$$

for a control bandwidth  $\omega_b$ , where:

$$K_p = c \cdot \omega_n^2 \quad (2.39)$$

$$K_d = 2 \cdot \xi \cdot \omega_n \cdot c - d \quad (2.40)$$

$$K_i = \frac{\omega_n}{10} \cdot k_p \quad (2.41)$$

and:

$$d = -N_r \quad (2.42)$$

For the surge controller,  $c$  is given by the difference between the vessel mass,  $m$ , and the added mass from water displacement in surge  $X_{\dot{u}}$ . Similarly, for the yaw controller, given by the gap between the moment of inertia  $I_z$  and added mass in yaw  $N_{\dot{r}}$ :

$$c_u = m - X_{\dot{u}} \quad (2.43)$$

$$c_\psi = I_z - N_{\dot{r}} \quad (2.44)$$

A damping ratio ( $\zeta$ ) of 0.8 was chosen considering Fossen (2023), as a lower damping ratio ensures a lower settling time in reaching satisfactory surge velocities and heading adjustments, albeit at the risk of larger oscillations before reaching a steady state response. With a control bandwidth ( $\omega_b$ ) of 0.4 rad/s, the resulting controller gains from pole placement and the practically determined values are given in Table 2.2 and 2.3.

Controller	Parameter	Value
Surge	$K_p$	14.39
	$K_i$	3.13
Heading	$K_p$	15.21
	$K_i$	1.86
	$K_d$	0.7

Table 2.2: Controller parameters by pole placement

Controller	Parameter	Value
Surge	$K_p$	12
	$K_i$	0.7
Heading	$K_p$	37
	$K_i$	4
	$K_d$	8

Table 2.3: Controller parameters by trial & error

## 2.5 Acoustic Underwater Localization

Acoustic localization is a widely used technology in maritime target tracking, requiring one transmitter with three or more receivers (Alcocer et al., 2006), as presented in Figure 2.3. The receivers are generally mounted beneath a surface vessel, or on separate vessels with a set or measured distance.

In acoustic localization, the time difference between when the signal is transmitted and the receivers receive them indicates the location of the transmitter. The distance is calculated with the velocity the sound travels through water, before these distances are triangulated, to find the transmitter's specific location relative to the receivers' mean location. The time of arrival of the signals is given by

$$d = VT \quad (2.45)$$

Where the speed of sound  $V$  is considered constant in depths less than 200 meters due to negligible water pressure differences, and the time interval  $T$  is the interval between each sent signal is received (Penas, 2009).

The distance  $d$  between the receivers and the target results in a triangulation problem as illustrated in Figure 2.3. By determining the distance between the transmitter and each receiver, triangles are formed between them and the target, which can be used in calculating the actual distance to the target (Penas, 2009). Similarly to the distance problem in equation 2.28, following Alcocer et al. (2006), the distance to the target in three degrees is computed by

$$d_i = \|p_i - p_c\| = \sqrt{(x_i - x_c)^2 + (y_i - y_c)^2 + (z_i - z_c)^2}, \quad i = (1, 2, 3) \quad (2.46)$$

In which the target location is denoted as  $p_c = [x, y, z]$  and each of the different receiver locations as  $p_i = [x_i, y_i, z_i]$ .

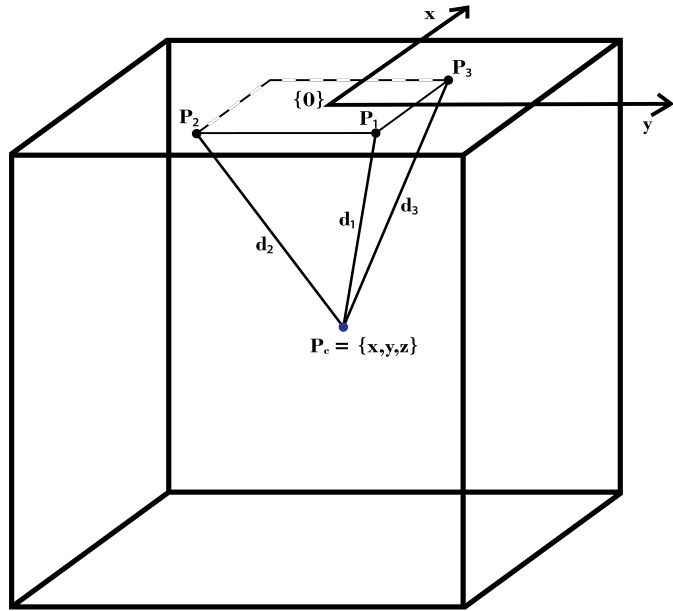


Figure 2.3: Underwater triangulation (*Illustration by Gresberg, Sigurd A.S., 2024*).

### Short Baseline system

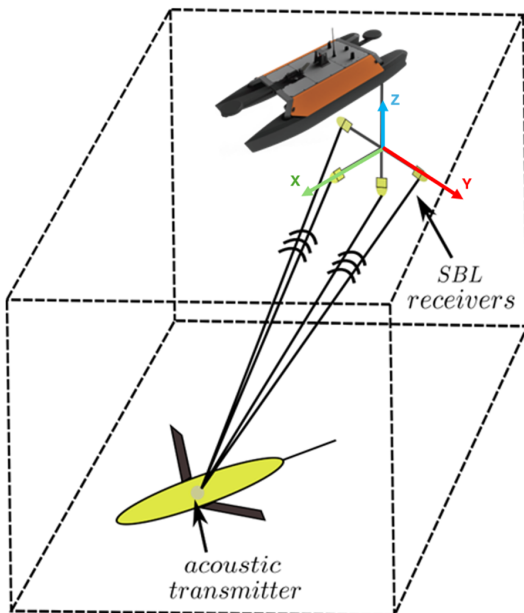


Figure 2.4: Concept drawing of acoustic transmitter-receiver relation.  
Saksvik et al. (2022).

A short baseline (SBL) system is an acoustic underwater localization technology, generally with a distance ranging between 1 and 100 meters between each beacon (Penas, 2009). Each beacon is an underwater microphone, located beneath a surface vessel or a rigid structure beneath the water surface. This provides the relative position of the target mounted with the sound transmitter by acoustic localization through triangulation, as showcased in Figure 2.4 (Saksvik et al., 2022).

# Chapter 3

## Materials

### 3.1 Otter USV Components

While the Otter USV frame is small, it is equipped with four 915Wh torqeedo lithium-ion batteries, optimized for extended operations for data acquisition in sheltered areas (Maritime Robotics, 2020). The USV supports radio, WiFi, and 4G communication and can be equipped with most relevant sensing technologies, depending on the project requirements. From the Otter USV illustration by Maritime Robotics (2024), The main components of the vessel are highlighted in Figure 3.1 and table 3.1.

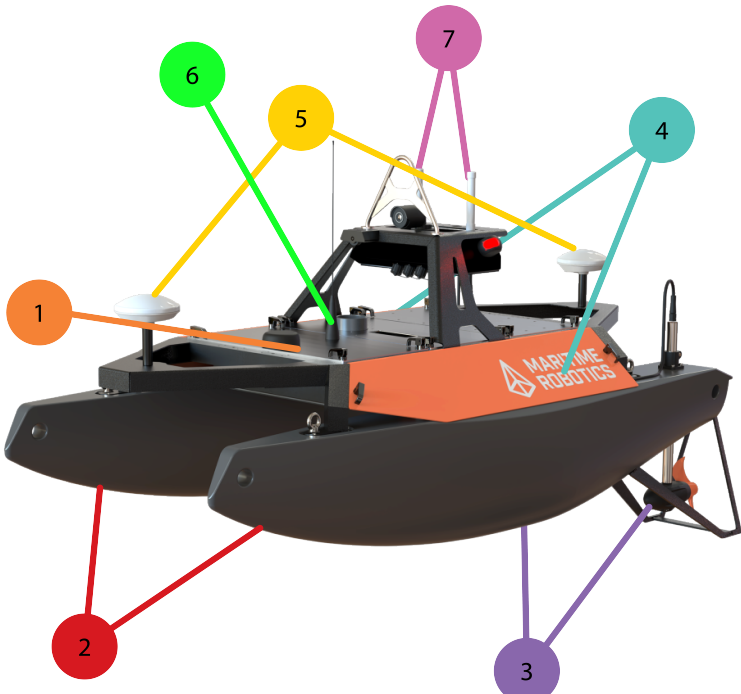


Figure 3.1: Otter USV assembled, numbered component list in Table 3.1.  
Maritime Robotics (2020).

No. (Figure 3.1)	USV Components	Component Description
1	On-Board system control box	Central unit of electronic systems
2	Pontoons	Floating structures for buoyancy
3	Torpedo thrusters	two electric motors up to 80HP
4	Side panels	Detachable side panels
5	GNSS dual antenna mounts	UBLOX NEO-M8
6	WiFi antennas	2.4GHz antenna
7	Radio antenna	5GHz MIMO radio

Table 3.1: Otter USV component list.  
Maritime Robotics (2020).

## On-Board System Control Box

The On-Board System Control Box (OBS), which contains the majority of the core sensors and electronics, is mounted on the front side of the Otter frame. This includes the On-Board Computer connected to the VCS, the AIS receiver with a high-frequency whip antenna, as well as an UBLOX NEO-M8 GNSS receiver and antenna (Maritime Robotics, 2020). It also holds a Huawei E3372H-153 4G LTE USB dongle and a WiFi interface with a 2.4GHz antenna.

## Inertial Navigation System

The OBS is also equipped with an SBG Ellipse2-D INS with RTK positioning, composed of an IMU and a dual antenna GNSS.

In RTK positioning, a base station is determined, and observational data is transmitted to multiple deployed receivers. Through this process, the relative position of the base station can be computed with high accuracy, given that the positioning data of the base station is accurate (Denys et al., 2017; Alkan et al., 2020). The IMU consists of gyroscopes, accelerometers, and magnetometers working in three axes, as well as temperature sensors, providing the altitude, heading, heave, pitch, yaw, roll, and navigational inputs (SBG Systems, 2023).

Additionally, the central processing unit of the INS applies a Kalman filter, a state estimation algorithm also known as linear quadratic estimation (Khodarahmi & Maihami, 2023). The Kalman filter initially completes a prediction formed from a series of state estimations, before these are integrated with previous data to perform predictions about the current and future system states. This process enhances the accuracy of system parameter estimates by minimizing noise, reducing positioning errors, and reducing variations in sensor readings due to dynamic changes in the environment. The INS is highly accurate, with an average positioning error of one centimeter and a heading error of 0.2° (SBG Systems, 2023). In practical application, the INS allows the vessel to accurately determine the inertial frame  $\{n\}$  position of the vessel, allowing for accurate calculations in the error between distance and heading to target.

## Communication Systems

Radio and WiFi were primarily utilized due to technical issues with the 4G dongle. As seen in Table 3.1, the radio is 5GHz, and the multiple-input multiple-output method is used to increase data capacity. Several signals can be simultaneously sent with multiple transmitting and receiving antennas, making it more reliable in areas with increased potential for disturbances (Martin et al., 2000). The Otter USV can also be utilized with an 802.11ac WiFi hotspot, with

a range of up to 400 meters, generally limited by the WiFi range of the users shore station device, which is any personal computer used to connect to the VCS and Otter USV. The IEEE 802.11ac is a wireless network standard in the 802.11 protocols, transmitting up to 1300Mbps (Cisco Systems, 2024). While having reduced interference from the surroundings and power demands from routers, it is able to reach high speeds by continuously switching between 2.4GHz and 5GHz.

## Vehicle Control Station

The VCS, a Thinkpad configured Ubuntu Linux, is provided with the Otter USV. The VCS features a graphical user interface, allowing a surveyor to plan and monitor tasks, displaying the USV position and surroundings for real-time monitoring at any given time, and additionally allowing for data acquisition of information regarding the vessel state. As the Otter is remotely controlled through the VCS, establishing a connection with the vessel via an alternative shore station requires the use of an application programming interface (API). This is necessary as the base system of the Otter does not permit direct communication with the vessel.

## 4G Connectivity

For deployments where the distance from the shore station to the vessel exceeds the maximum distance at which the radio or WiFi can be utilized, a Raspberry PI with a 4G connection was developed and installed on the vessel. The device routes all port specific incoming and outgoing network traffic to the vessel, which allows a connection to the vessel through 4G. To access the vessel from a remote network or machine, a virtual private network from ZeroTier (2024) must be installed on the remote machine and connected to the Otter USV virtual network.

## 3.2 Implemented Sensor Systems

Two different bracket systems were implemented in this project. One acoustic sensor and one optical communication device as depicted as 2 and 3 in Figure 3.2.

No. (Figure 3.2)	Implemented Systems	System Description
1	G2 Topside	Central unit of electronic systems
2	Optical Modem	Optical communication to underwater target
3	G2 Antenna	SBL Acoustic receiver

Table 3.2: Sensors implemented to the Otter USV

### 3.2.1 Water Linked Underwater GPS G2

Water Linked Underwater GPS (UGPS) G2 is a robust acoustic positioning system that is based on an SBL system. The setup is composed of the G2 Topside, G2 Antenna, and U1 Locator.

The acoustic sensor consists of one transmitter and four receivers, where the transmitter produces a sound signal within frequencies accepted by the receivers to calculate the relative location of the target with respect to the antenna. This data can be extracted with the API from Water Linked AS (n.d.-b).

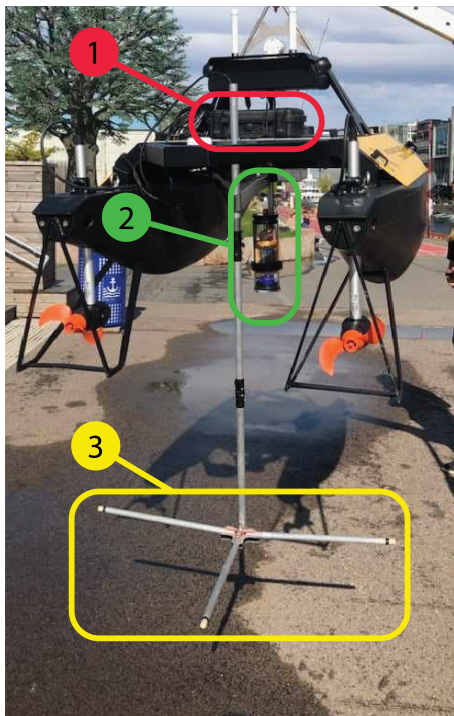


Figure 3.2: Assembled Optical Modem and Acoustic Antenna.

## G2 Topside

The microcomputer, GPS, and battery pack are located within the G2 Topside, on top of the vessel in Figure 3.2, denoted as number 1. The G2 Topside computes the calculations for the time of arrival and triangulation.

Communication with this unit is done via WiFi to a local device. This device may access the data through the graphical user interface with the web address; <http://192.168.7.1/>, set up by Water Linked, or with custom scripts through the API (Water Linked AS, n.d.-b).

## G2 Antenna

Water Linked's G2 Antenna has four acoustic transducers as receivers. It accepts sound frequencies ranging between 31.25 and 250 kHz, most often used at 200 kHz. Each receiver is omnidirectional, with the communication to the G2 Topside done through an Ethernet cable. The antenna has a size of 151 x 98 x 53.5 cm while extended (Water Linked AS, n.d.-a), and is placed on the back-side of the Otter frame, depicted in Figure 3.2 and denoted as number 3.

## U1 Locator

The U1 Locator, exhibited in Figure 3.3 (Water Linked AS, n.d.-c), is the acoustic transmitter of the system and is attached to the target. The component has a pressure sensor, with a depth rating of up to 300 m and an operating temperature from -10°C to 60°C. The maximum range is 100 to 300 meters, depending on where the focus is set in the GUI, with a battery life of up to 10 hours (Water Linked AS, n.d.-a).



Figure 3.3: Acoustic transmitter.  
Water Linked AS (n.d.-c).



Figure 3.4: Attachment of the optical sensor.

### 3.2.2 Attaching the optical modem

Although practical implementation of the optical modem for communication is not completed in this project, the attachment solution in Figure 3.4 was a practical, low cost, and efficient solution to connect the modem to the USV in preparation for further research. The placement is exhibited in Figure 3.2 in box number 2.

### 3.2.3 Mechanical Design for Acoustic Sensor Holder

The acoustic sensor was previously attached by using disposable zip-ties, thus a solution with improved ease of use and less waste was necessary. Due to the damping effects in aquatic conditions, a strong, but cost-efficient material was required. Additionally, due to planned use in the ocean, the sensor brackets must be resistant to saline and slightly acidic solutions. High stability is also needed to ensure precise data acquisition, while ease of operation at sea from a nearby boat or dock must be maintained.

### 3.2.4 Choice of Material & Printing Technology

Testing models from polylactic acid were 3D printed by Fused Deposition Modeling (FDM). Whereas polylactic acid is a cost-efficient testing material for designs, it is not suitable for extended exposure to saltwater and UV-light, nor recommended for functional or industrial

parts (Montalvão et al., 2020; Kafle et al., 2021). Acrylonitrile styrene acrylate (ASA) filament was a more fitting material for this, though requires the use of FDM printing, which gives low resolution, design complexity, and weakness between layers of the print (Cao et al., 2020). This suggested the use of nylon with a Selective Laser Sintering (SLS) printer, where nylon powder is fused together and gives roughly the same strength across the whole part proportional to the cross-section (Asada et al., 1976).

## Selective Laser Sintering and Nylon 12

SLS has the overall highest performance of the aforementioned choices with respect to achieving omnidirectional strength and higher design complexity (Kafle et al., 2021). The available material for OsloMet's SLS 3D printer was Nylon 12 from FormLabs, which is slightly hydrophilic with up to 2% water absorption, but also water-repellent. Although Nylon 12 does not deteriorate with prolonged water exposure, as the properties may slightly weaken until dehumidified, coating the material in acrylic or silicone-based marine paint could be done to counteract water absorption (Asada et al., 1976).

## Fused Deposition Modeling With Carbon Fiber and Nylon-Carbon Fiber

While regular FDM printing has weaknesses in torsion and axial tension along the print orientation, this technology provides good compression and high planar strength when also combined with carbon fiber, and nylon-carbon micro fiber composite filament compared to the aforementioned SLS with Nylon 12 (Melenka et al., 2016; Kafle et al., 2021). MarkForged MarkTwo is a 3D printer with these qualities, which was available at OsloMet (MarkForged, Inc, 2024).

### 3.2.5 Choice of Design

The design of the fastener derives from a need for stability and ease of operability. The result is a clamp operated by a winged nut on a T-lever bolt, as seen in Figure 3.5. The rod support was mainly produced to relieve torque on the clamp, but also to reduce inertia and oscillation that would otherwise occur with only a short clamp attached at the top of the rod which would give imprecise readings for the UGPS.

### First iteration with testing

After working through initial versions of a clamping system with polylactic acid, the first iteration of was completed. The initial design focused on motion in the positive x-direction only, as the initial control system only allowed the vessel to apply forward thrusts, resulting in a critical fracture during a test, in both the clamp and rod support. This was likely due to unexpectedly high damping forces from water displacement, while these forces were not uniformly applied against the surge direction. Additionally, some zip-ties to fix the antenna in place were used, which could have placed the SBL acoustic sensor slightly askew. The cross-section of the rod support was also quite thin, where an increased size could have improved component strength.

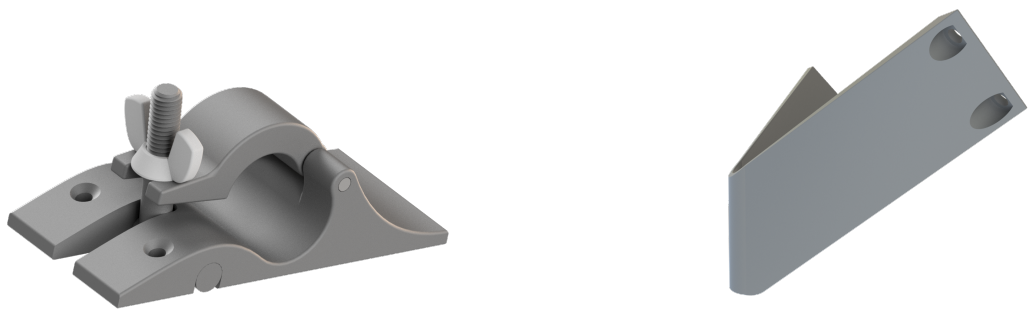


Figure 3.5: Rendered 3D model of the acoustic sensor's clamp and rod support.

The SLS printing bed was also a limiting factor to the size of the rod support, where the maximum available space was used. Therefore, to increase the rod support size, a bigger print bed was required.

### Second iteration

Considering the initial iteration flaws, the cross-section around the bolt holding the clamp was thickened. Furthermore, where the previous rod support was designed for only withstanding forces in the negative x-direction, the second iteration improves on resisting drag from water by providing support in all directions on the horizontal plane, illustrated in Figure 3.7. This iteration was also 3D printed in an FDM printer, with nylon 12 with micro carbon fiber filament and layers of continuous carbon fiber filament, as shown in Figure 3.6. The second iteration is expected to provide a significant improvement in its structural strength and durability, given that it exhibited hardly any flex when the vessel was partially lifted from the ground by the rod support.

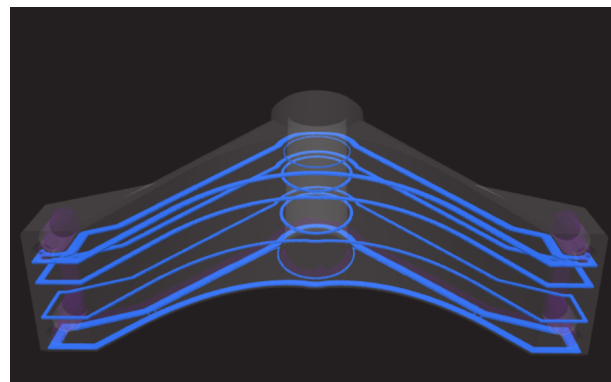


Figure 3.6: Illustration of carbon fiber layers in the rod support.

The final mounted clamp system is illustrated in Figure 3.8.



Figure 3.7: Rendered 3D model of the acoustic sensor's clamp and rod support second iteration.



Figure 3.8: Assembled clamp system for the acoustic sensor.

# Chapter 4

## Methods

### 4.1 System Design

As depicted in Figure 4.1, The implemented control system builds on an API handling the communication with the Otter USV, performing calculations on the current state of the vessel through the USV's sensors. Both PI and PID controllers were implemented, sequentially controlling the USV's surge and heading, based on the guidance model in the API. The surge controller signals were parsed through the control allocation to ensure the physical response reflects the desired thrust in surge and yaw.

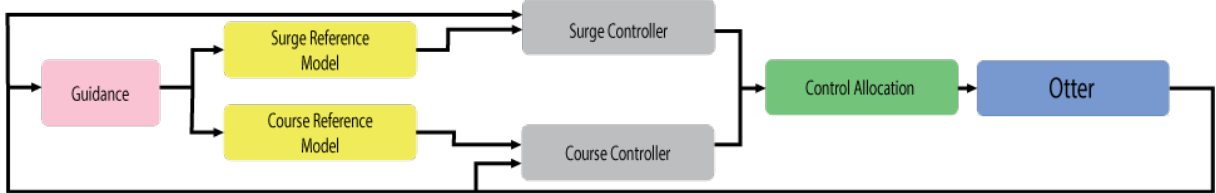


Figure 4.1: Otter USV Control system.

### 4.2 Application Programming Interface

To handle communication with the Otter USV, an application programming interface was developed and employed as an external script in the target tracking software. This API extends and enhances the functionalities documented in Kjelsaas (2022) and Gresberg et al. (2023).

The API was developed using an object-oriented approach, resulting in a class that can be imported into external scripts, creating easy-to-access functions and sensor data. This design was chosen for its adaptability and reusability, with ease of integration and expansion in future development and research. The main class `otter()` contains the necessary methods for establishing a connection, updating sensor values, and sending control signals to the vessel.

Listing 4.1: Otter API: Connector

```
class otter():
    def establish_connection(self, ip, port):...
```

```

def close_connection(self):...
def update_values(self):...

```

## Otter Communication

To interact with the Otter USV, a connection must initially be established. This can be achieved by calling the `establish_connection()` function in Listing 4.1 with the correct IP address in string format and port in integer format, as seen in Table 4.1. Once a connection is established, it will stay connected until either a signal loss occurs or the function `close_connection()` is called. The establishment of a reliable connection ensures continuous data exchange between the vessel and the control software.

Connection method	IP address	Port
WiFi	10.0.5.1	32001
Radio	192.168.53.2	32001
4G	100.6437.13	32001

Table 4.1: Otter USV communication methods

The sensor data, along with some locally calculated values, are stored in the `otter.sorted_values[]` dictionary. By calling the `update_values()` function in Listing 4.1, the dictionary is updated with the latest sensor data from the Otter USV, while also updating the locally calculated values in the dictionary, such as the inertial frame  $\{n\}$  position from the observer coordinates. The function is integral to maintaining an accurate representation of the vessel current state, such as position and velocity. In all tests, the function was executed in every control cycle, amounting to 10Hz, ensuring precise data at all times in decision-making processes.

## Control Signals

The API provides two main functions designed to handle raw control signals when sending signals to the thrusters from an external controller. Additionally, several smaller functions can be individually used to perform specific calculations required to convert control signals from controllers to those transmitted to the Otter USV.

Listing 4.2: Otter API: Control

```

class otter():

    def controller_inputs_torque(self, tau_X, tau_N, on_linux):...

    def controller_inputs_radS(self, n1, n2, on_linux):...

```

The two main control functions are listed in 4.2. The `controller_inputs_torque()` function accepts control signals in the form of torque in the surge and yaw directions, represented by the `tau_X` and `tau_N` arguments. The `controller_inputs_radS()` function requires control signals as rotational speed for each thruster in radians per second, similarly represented by the `n1` and `n2` arguments.

Calling either of these functions will handle the control allocation, throttle interpolation, and transmission of the calculated values to the Otter USV, provided there is an established connection. As discussed in section 2.2, the control allocation is detrimental in determining how the

desired forces are distributed among the thrusters, ensuring accurate thruster outputs. Throttle interpolation prevents abrupt changes in the thruster inputs, ensuring smooth transitions and improving the system's stability. Both of these functions include the "on\_linux" argument, which defaults to False. When running in a Linux environment, this should be set to True to prevent issues with the throttle interpolation.

## 4.3 Simulator Development

For the initial development and tuning of the guidance and control system, the modified version of the simulator by Fossen (2023) was employed. Originally, the simulator featured a library with multiple vessels which could be selected from the start menu and then simulated. The original simulator was developed to simulate heading controllers without changes in surge, resulting in the simulator only containing a linear yaw controller. A constant force would be applied to the surge direction, which would be parsed through the control allocation to attain the desired thruster speeds.

The Otter USV and dynamics simulation sections of the simulator were extracted and adapted together into a standalone Python program, which could be easily implemented with other scripts. The code was modified to implement external controllers, in both the yaw and surge direction, where real-time values such as velocity and heading can easily be accessed. This enabled the controllers to be applied in both the simulator and the practical target tracking, resulting in more consistent and realistic simulator results.

Due to the original simulator only featuring heading control guidance, multiple new target types were introduced and implemented. Different targets moving in a straight line and a perfect circle were put into practise, as well as other target paths with higher demands to the heading controller, such as a square. Within the options portion of the source code, multiple parameters affecting how the target behaves can be tuned to achieve the desired target behaviour. This includes customizing which path the target should follow, the circle radius, or having the target move in a set path with different velocities and coming to a complete stop at the end of its path.

## 4.4 Practical PI and PID Implementation

### 4.4.1 Throttle Map

Although possible throttle control signal inputs to the USV are within the range  $-1.0 < u < 1.0$  in surge and yaw, it was found that low values exerted unexpectedly low rpm outputs, while any value within the interval  $-1.0 < u < -0.6$  and  $0.6 < u < 1.0$  would always produce a uniform maximum rpm when attempting to reach a desired location. Simply using control signals bounded by  $-1.0 < u < 1.0$  could therefore produce imprecise regulation of velocity, as moderate control signals would produce a significantly higher rpm than expected or desired, ultimately leading to overshooting or struggles in heading correction.

A throttle map was created through logs of produced rpm for specific surge and yaw inputs, concluding that the control signals created a non-linear output rpm. By enabling the controllers to call on desired rpm values from a CSV file in the  $-0.6 < u < 0.6$  range rather than  $-1.0 < u < 1.0$ , a pseudo-linearization of the control signals was achieved, improving the controller stability, reducing overshoot and oscillation. The initial throttle map, presented as

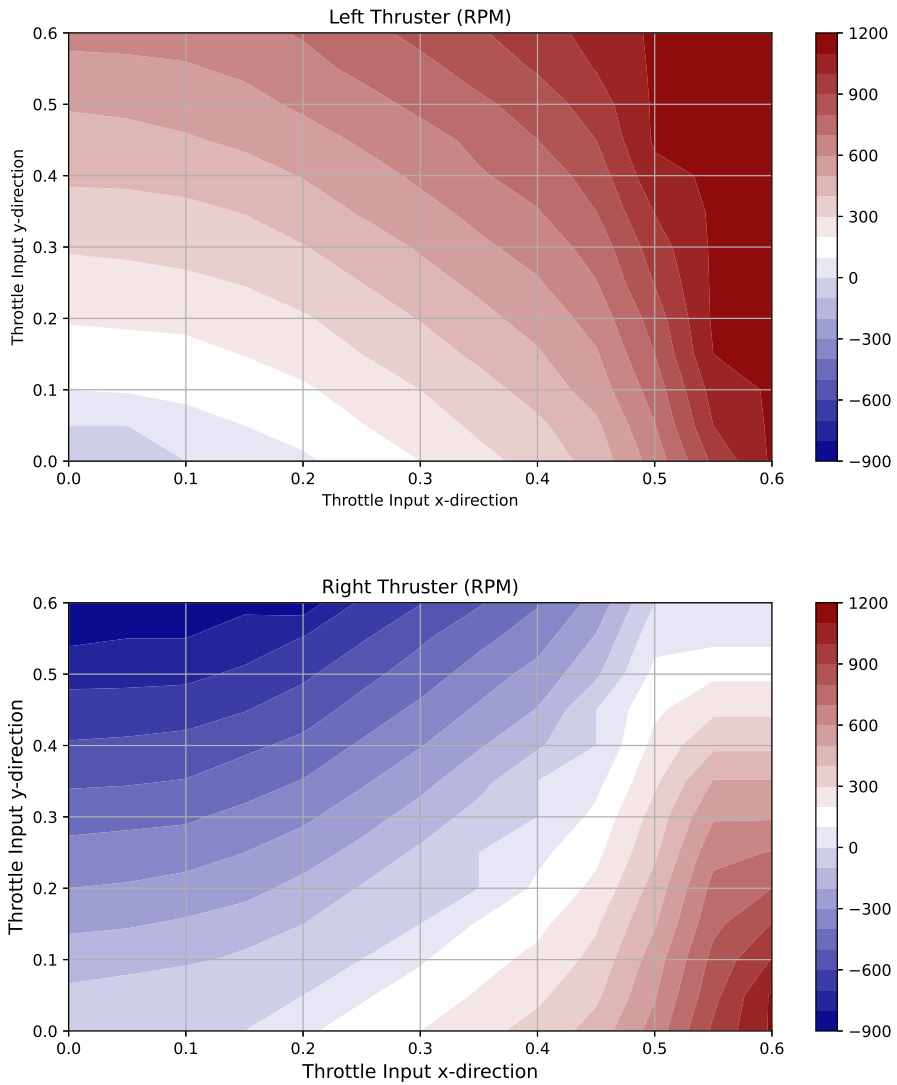


Figure 4.2: RPM from throttle control signal in left and right thrusters.

a plot in Figure 4.2, only used inputs in the north and east directions. However, negative and positive control values were discovered to share the same relationship between input control signals and output rpm, and could thus uniformly be used for inputs in any direction.

### Surge output regulation

In addition to using pure PI and PID controllers only employing the PID control laws for surge (2.36) and yaw (2.37), other methods were implemented to regulate the controllers' outputs. A function was added to limit the total force the controllers could apply to the Otter USV, with stricter limitations in the yaw controller. The Otter USV is allowed a total force of 200 Newton (N) that can be applied at any given moment. This force is divided between the controllers, with a maximum of 200N for surge and 115N for the yaw controller. The force applied by the yaw controller is subtracted from the total force before being applied to the Otter USV.

$$\Sigma_{\tau} = 200N - \tau_6 \quad (4.1)$$

The remaining amount of the total force  $\Sigma_\tau$  is made available to the surge controller, as a limit to the force which can be applied to the Otter USV in surge simultaneously with the yaw direction:

$$\tau_1 \leq \Sigma_\tau \quad (4.2)$$

In the surge, the PI controller was modified with a function scaling down the output depending on the yaw error, by calculating a yaw error scalar and multiplying the output with the scalar:

$$\gamma_\psi = \frac{e_\psi}{\pi}, \quad -\pi \leq e_\psi \leq \pi \quad (4.3)$$

Where  $\gamma_\psi$  represents the yaw error scalar, and the surge force is computed to:

$$\tau_1 = \tau_1 \cdot (1 - |\gamma_\psi|) \quad (4.4)$$

This resulted in the surge controller significantly reducing the output in cases where the yaw error is large, reducing the travel distance away from the target before the desired heading is reached.

### **Integral cap and reset**

Early tests determined that if reaching the desired heading or the desired target radius was not done within a short duration, the controllers would become aggressive due to the integral portion of the controller building, infinitely increasing with time. This would ultimately result in overshooting the target and oscillating around it.

To resolve this issue, an integral cap and an integral reset function was introduced to the controllers. The integral cap was determined by the physical response from the system, resulting in a cap of 10 in the surge PI controller and 40 in the yaw PID controller. The integral reset function was triggered when the respective controllers hit their respective targets within a set threshold. The physical responses of the system deemed this to be within 1° heading error in the yaw PID controller and within the set target radius in the surge PI controller. This resulted in more stable control outputs and a significant decrease in overshoot.

### **Negative thruster rotation**

The Otter has a built-in time delay when changing thruster directions. The delay before the rpm changes in an already active thruster is less than a second, with the time constant to reach approximately 63% of the steady-state response after a step input, is one second. However, when the thrusters are inactive or changing directions, this process takes up to three seconds. This is an implementation by either Maritime Robotics or Torqeedo as to protect the thrusters from mechanical stress due to inertia and momentum.

Due to the significant time delay, the thrusters were initially set only to receive input signals in a positive surge direction. Although reducing the speed heading adjustments of the vessel, by ensuring all control signals have the same time constant, the controller is more predictable. Additionally, in situations where the heading error is large, there is no significant delay where the target is moving further away from the vessel. This also inhibits unwanted reversed movement,

preventing the need for any other functions and ensuring positive velocities. It was, however, discovered that this negatively impacts the USVs' capabilities in following the target in cases of overshooting, primarily due to the increased time required for heading adjustment, which would require the vessel to completely circle around the target.

#### 4.4.2 Practical PI and PID Gain Adjustment

In addition to pole placement, an empirical trial-and-error approach was employed to practically identify the optimal PI and PID gains. Simulations were conducted in circular and straight-line target tracking, as well as for scenarios requiring rapid heading adjustments greater than 90°. In these simulations the gains were adjusted to minimize the average distance from the target over the duration of the test. The obtained values were applied in a practical setting, where further optimizations were completed. The final gain values in the surge PI and the heading PID controllers from practical adjustments are presented in Table 2.3. As seen in Tables 2.2 and 2.3 the PI surge controller by the two methods had relatively similar gains, however the heading controller gains in the empirical methods were much higher, especially in the  $K_d$  gain.

### 4.5 Underwater GPS G2 Program Implementation

To receive and use the data from the UGPS G2 there was implemented a Python program using the system's API. This was based on the Water Linked GitHub demo (Water Linked AS, 2017).

The program obtains the distances in the x-, y- and z-axis in relation to the antenna's location and direction. Thereafter, this gets logged into a CSV file at 5Hz, which can later be plotted to illustrate the location of the target related to the antenna. This would preferably be sent as data directly to the shore station, to handle the data for use in live target tracking cases.

### 4.6 Testing Procedures

Ice formation around the docks and traffic from cruise ships and the royal yacht "Norge" around the Oceanlab OsloMet created difficulties in the early practical deployment of the USV. The practical tests were initiated in early March 2024.

#### 4.6.1 Initial Testing Procedure

The initial practical tests were executed in the harbor outside the Oceanlab, as seen in Figure 4.3. Otter can easily be deployed by the steps at Fontene Tjuvholmen, while the waterfront around the bay provides some coverage from wind, waves, and other noise from boat traffic.

Through the preliminary and early testing of the USV, understanding and optimization of specific functions was prioritized, including:

1. *Testing input signal to thruster response.*
2. *Practical parameterization of the PI, and PID controller gains.*
3. *Ensuring comparability between simulated and physical results.*
4. *Troubleshooting.*



Figure 4.3: Testing site of initial practical tests, Fillipstadveien 7, 0252 Oslo.  
(Google Earth, 2024a).

These trials mainly consisted of operations in straight line and circular target tracking, though the test site is confined, making it difficult to evaluate how the USV would operate in open sea conditions, without larger limits on maneuverability.

Before progressing to the open sea tests, an evaluation of the different communications systems, primarily WiFi and radio, was done to ensure continuous connection to the USV. Additionally, the consistency and accuracy of the vessels, such as velocity and position, were verified.

#### 4.6.2 Final Testing Procedure

The final testing procedure was divided into two main cases, each using a simulated target for the USV to follow:

- *Case 1*: investigates the USV capabilities in straight line target tracking, with a starting position directly east of the target start position.
- *Case 2*: has the target continuously moving in a circular motion with a radius of 40 meters.

By appraising the USV's capability in the two cases, the core functions of the surge and heading controllers are considered. Its ability to follow a straight-line target evaluates if the surge controller is able to reach the required velocities in an acceptable time frame without overshooting the target. Additionally, with a starting position at a significant distance from the target, the yaw controller must adjust for any heading errors. Similarly, the circular target test requires constant heading adjustments from the Otter, displaying the heading controller's ability to track the target without oscillating around it. Both cases were tested using controller parameters from pole placement and values determined practically through previous testing to

ascertain if the calculated parameters yielded an improved result.

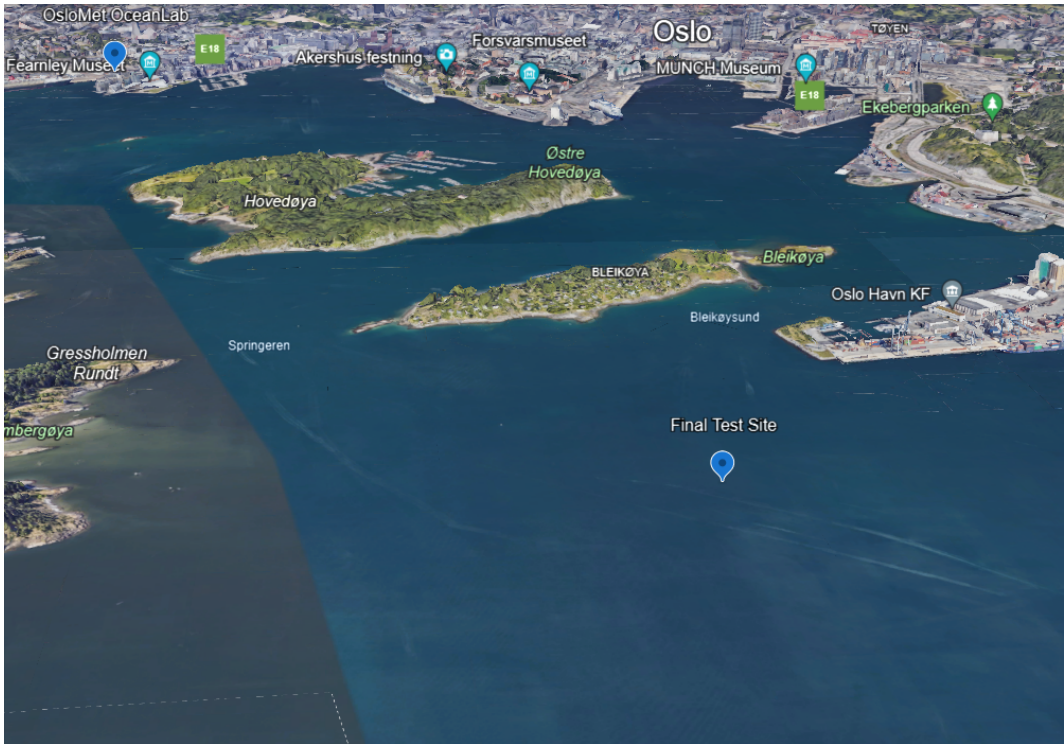


Figure 4.4: Testing site of final practical tests, between Gressholmen-Rambergøya and Sjursøya in the Oslofjord.

Google Earth (2024b).

The final tests were conducted in late April between Gressholmen-Rambergøya and Sjursøya, displayed in Figure 4.4. By deploying the USV in open water, it was possible to test over larger distances without being inhibited by traffic or other constraints near the docks. This also allows for the Otter to be tested at higher speeds due to its max speed of  $u \approx 3m/s$  exceeding the 5 knots limit near the shoreline. Due to low traffic and good weather conditions, disturbances from wind and waves were mostly negligible during the test.

# Chapter 5

## Results

This chapter details the results of the study on the Otter USV’s target tracking system. Initial test results which lead to major system modifications are discussed before the final results are presented. The practical deployments were done using both the determined pole placement values, and the values determined by practically adjusting the gains during earlier simulations and tests. The simulation results for the same cases are also presented, as these are compared with the practical results.

### 5.1 Initial test results

Initial tests showed a significant discrepancy between the simulator and actual performance. The simulations had the USVs starting position at a significant distance from the moving target, with the heading error being small, granting larger distances to compensate for negligible heading errors. When attempting to track targets close to the starting position with a negative x-direction between the target and the body-frame  $\{b\}$ , the controls would prioritize backward movement over heading correction. The USV was also prone to overshooting the target, especially struggling in circular movements, largely due to issues with non-linearity in the thruster signals. This had a cumulative effect on the still-moving target, leading to sub-optimal tracking and large oscillations around the target path.

The main issues of non-linearity in control signals were solved by the implementation of the interpolation functions and throttle map, as well as the rate limiters to the integral portion of the controllers. By the implementation of the throttle map the control signals are therefore given as a desired rpm, rather than a control signal between  $-1 < u < 1$ , making it easier to analyze the physical response of the system. By demanding a considerable error in the heading angle before allowing reverse thrust, excessive reversed movement is prevented, and the controller could regulate the heading with less erratic behaviour.

### 5.2 Case 1: Straight Line Target Tracking

In *Case 1* the USV was set to track a target moving in a straight line at a constant velocity of 1.4 m/s. The starting position of the USV was directly east from the target, with the target continuously moving until oscillation around the target significantly dissipates.

### 5.2.1 Simulated Results

In the simulated straight line target tracking, depicted in Figure 5.1, the vessel has its starting position 10 meters directly east of the target start position. At the beginning of its travel the target overshoots the target by almost 35 meters before changing its heading and reaching the target path without any significant oscillations. While the overshoot is significant, the vessel is able to reorient itself and closely follow the target until the end of the path, with an average distance of 6.8 meters to the target throughout the simulation.

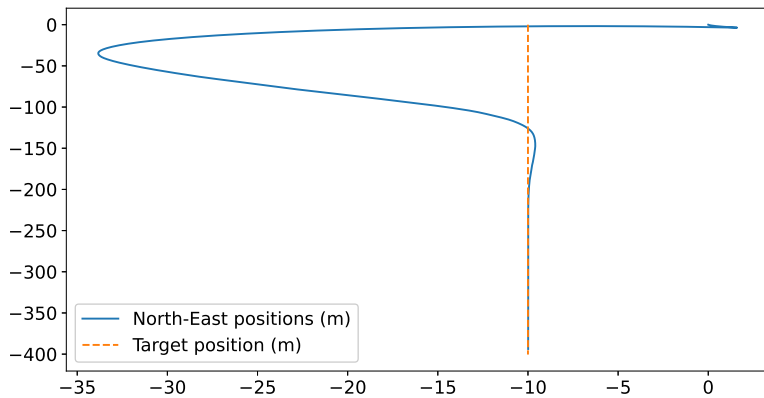


Figure 5.1: Simulated straight line target tracking - Target and vessel path - Pole placement gains

### 5.2.2 Practical Tests

#### Pole Placement Gains

For the pole placement gains in case 1, the target displays a more inconsistent behaviour than in the simulations. As displayed in Figure 5.2, the vessel is still overshooting the target, though adjusting its heading much earlier which could indicate that the USV experiences higher damping forces than what is modeled in the simulator, ultimately reaching a lower max velocity. The USV also needs longer before stabilizing around the target path, though the deviations away from the target is seen to be minimal, generally staying within the determined target radius after the 150 meter mark.

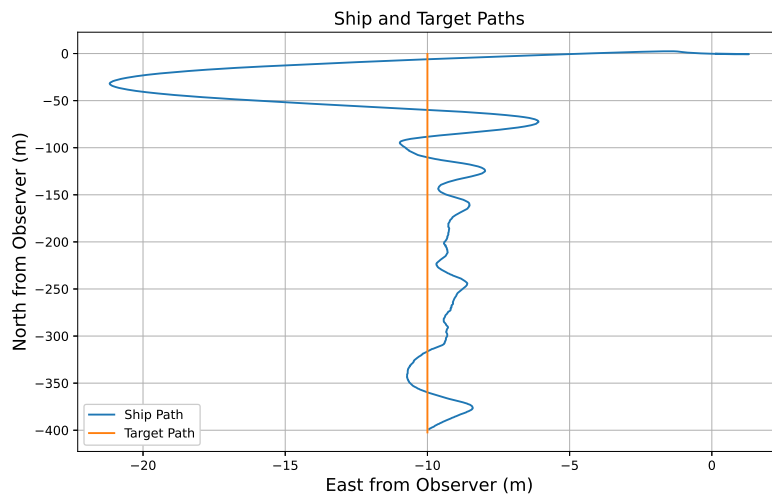


Figure 5.2: Straight line target tracking - Target and vessel path - Pole placement gains

The control signals in Figure 5.3 display how most major corrections in the heading were completed during the first 50 seconds of testing, before the vessel stabilized and more consistent control signals were observed. Similarly the velocities in Figure 5.4 equivalently show the Otter USV increasing its surge velocity in the initial stages to reach the target, after which the average speed is similar to that of the target.

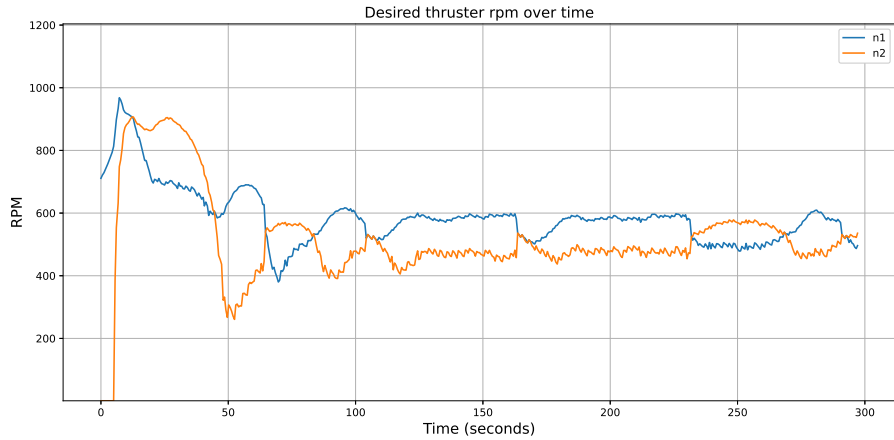


Figure 5.3: Straight line target tracking - Control signals - Pole placement gains

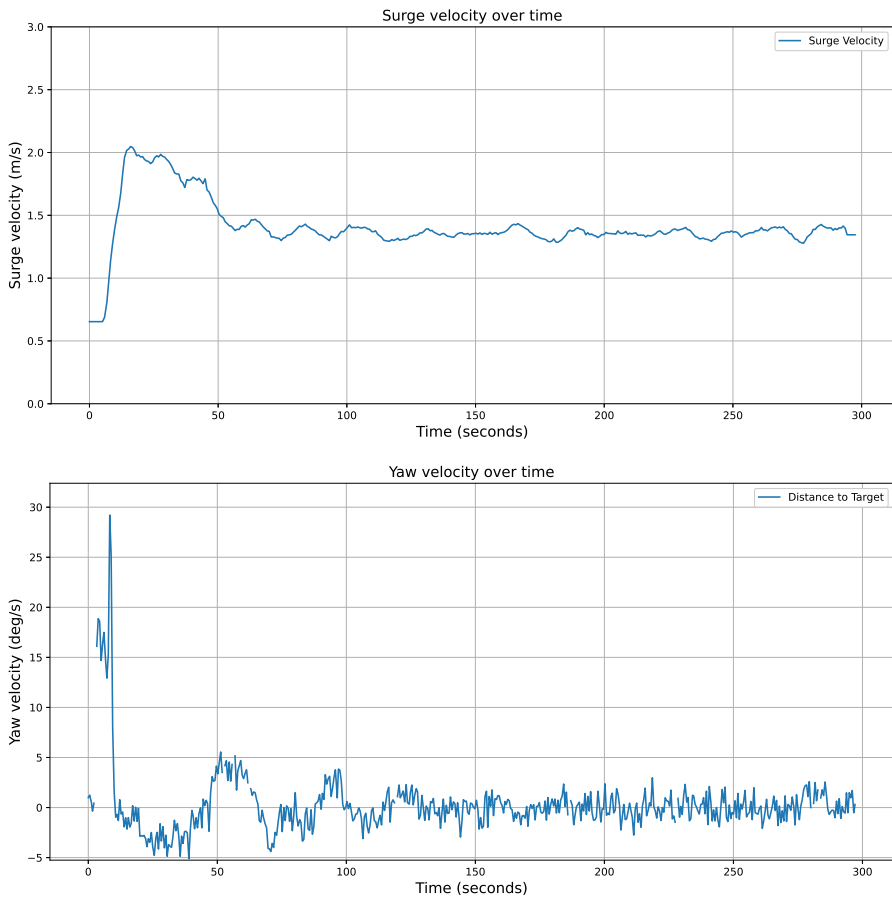


Figure 5.4: Straight line target tracking - Surge and yaw velocity - Pole placement gains

### Trial and Error Gains

Utilizing the gains from Table 2.3, the straight line target tracking presented in Figure 5.5 result in a much smoother response, gradually adjusting the heading to intercept the target. The vessel reaches the target around 25 meters earlier than by pole placement before continuously following the target closely within the set target perimeter.

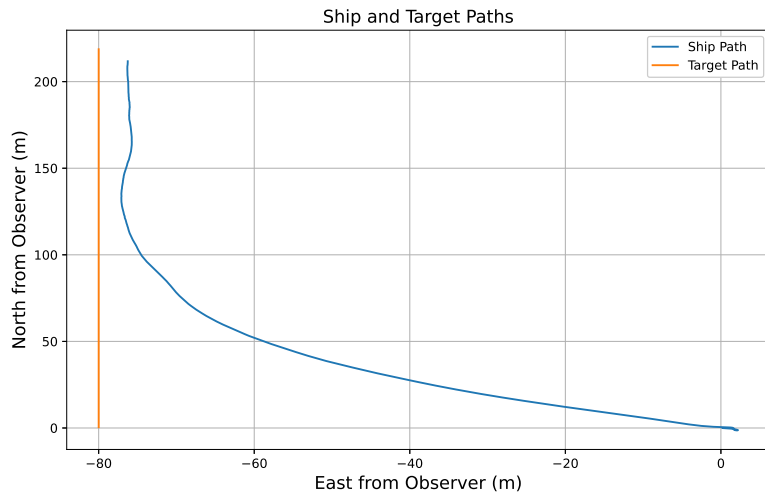


Figure 5.5: Straight line target tracking - Target and vessel path - Trial and error gains

An aggressive adjustment is made in the initial stages as the vessel is oriented away from the target path, seen by the control signals in Figure 5.6, before a gradual decrease as the vessel is close to reaching the target. This resulted in no overshoot and a smooth transition from catching up to the target, to tracking and following the target at the target velocity and heading. The same relationship is seen in the velocities in Figure 5.7 with major heading adjustments in the first ten seconds.

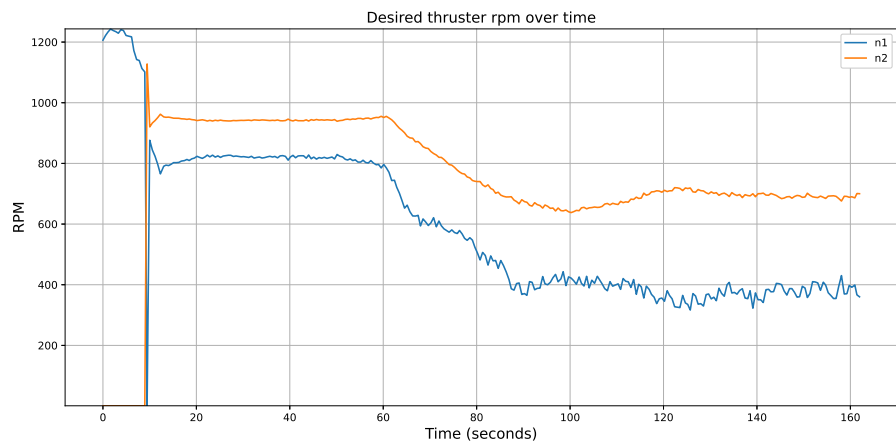


Figure 5.6: Straight line target tracking - Control signals - Trial and error gains

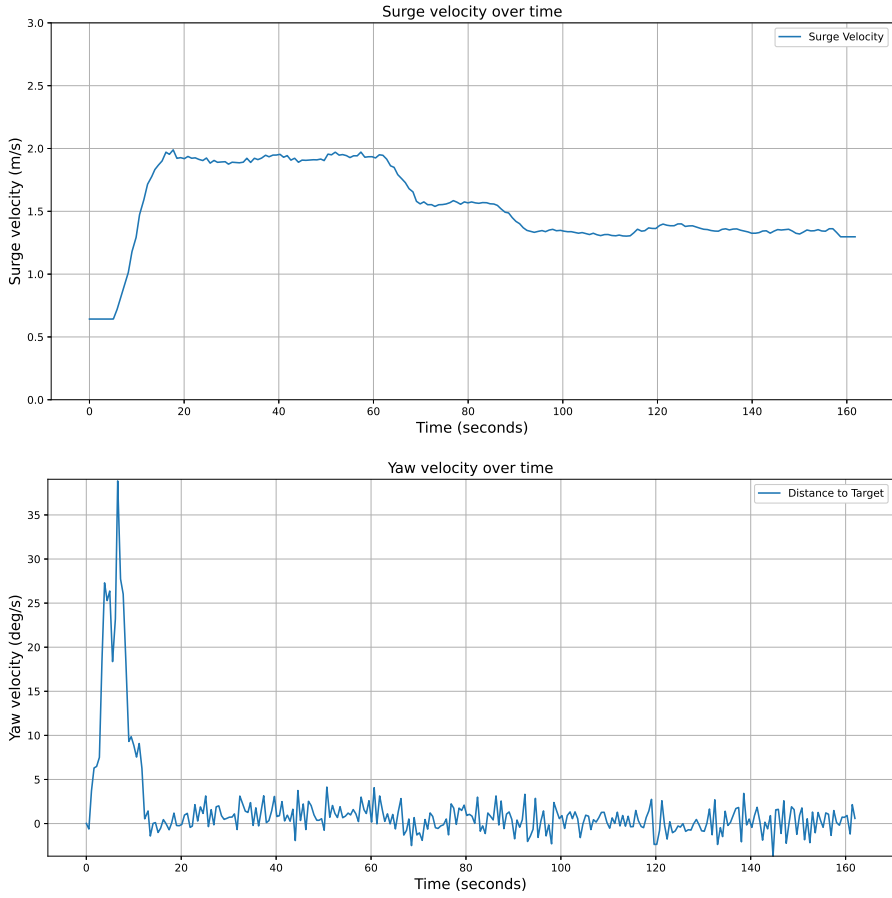


Figure 5.7: Straight line target tracking - Surge and yaw velocity - Trial and error gains

### 5.3 Case 2: Circular Target Tracking

In Case 2 the USV was set to track a target moving clockwise in a perfect circle with a radius of 40m. The starting position of the USV was south-east relative to the starting position of the target.

#### 5.3.1 Simulated Results

In the simulated circular target tracking, exhibited in Figure 5.8 and 5.9, the target was initially moving in the direction of the vessel eastwards. The vessel intercepted the target and passed it approximately 15m north and 5m west relative to the starting position of the vessel, slightly overshooting the target. While the target continued moving away the controllers performed significant heading adjustments to reorient itself towards the target path. After again reaching the target, the vessel adjusted its velocity and closely followed the target path throughout the simulation. The pole placement and the trial and error gains resulted in close to identical results, except for a small overshoot when reaching the target path while employing the calculated gains.

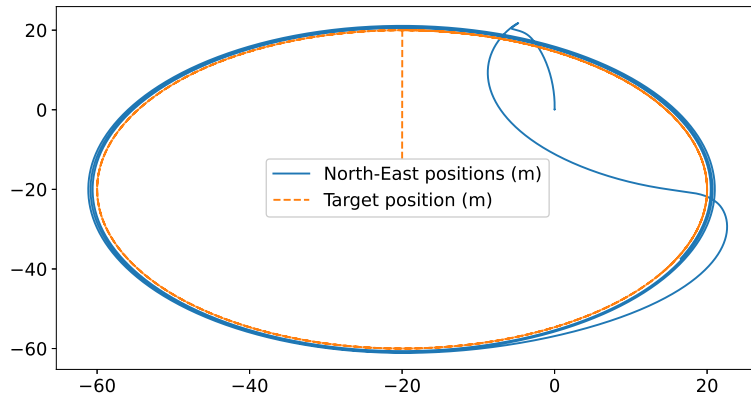


Figure 5.8: Simulated circular target tracking - Target and vessel path - Pole placement gains

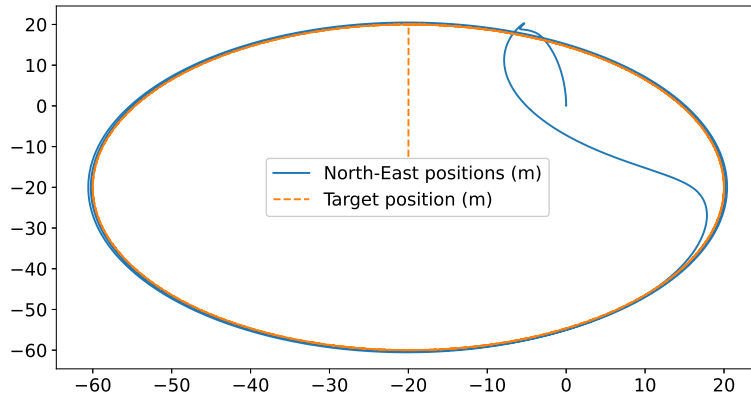


Figure 5.9: Simulated circular target tracking - Target and vessel path - Trial and error gains

### 5.3.2 Practical Tests

#### Pole Placement Gains

The path in Figure 5.10 indicates a somewhat similar response and behaviour to that of the simulation in the initial stages of the practical test, with the target being intercepted, followed by an aggressive heading adjustment to catch up to the target. Some variance is seen once the vessel caught up to the target, with the vessel approaching the target path multiple times, slightly sliding away to either side of the target path, before catching up again.

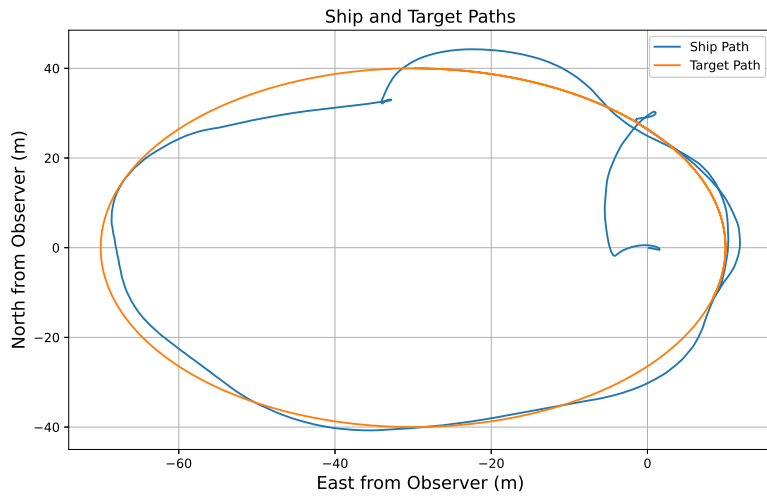


Figure 5.10: Circular target tracking - Target and vessel path - Pole placement gains

After the target travelled for close to 200 seconds, the vessel slightly overshoots, resulting in the vessel performing substantial heading adjustments before returning to the target path. Slightly before reaching the top northern position at the 200 second mark, the vessel readjusts its heading, which might be attributed to the impact angle of incoming waves pushing the vessel out of position. This behaviour is also exhibited in Figure 5.11 and 5.12, however the velocity uptick around the 200 second mark is quite significant, at close to the vessels maximum velocity. The control signals are also erratic, indicating that the heading controller gains might be too low in open sea conditions.

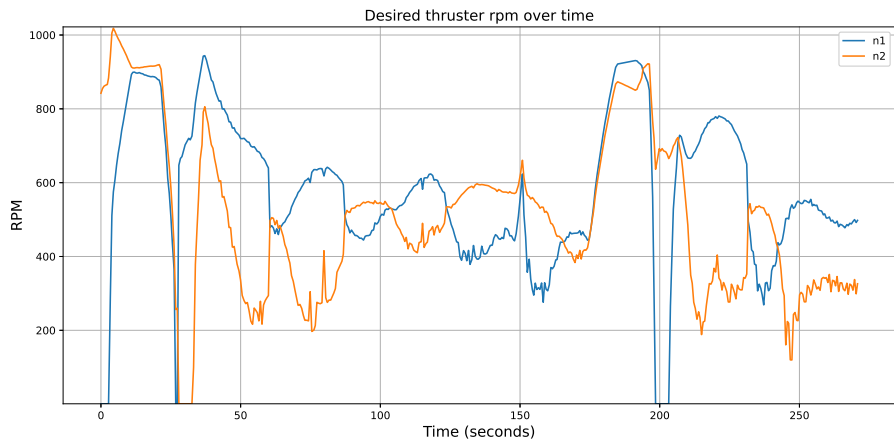


Figure 5.11: Circular line target tracking - Control signals - Pole placement gains

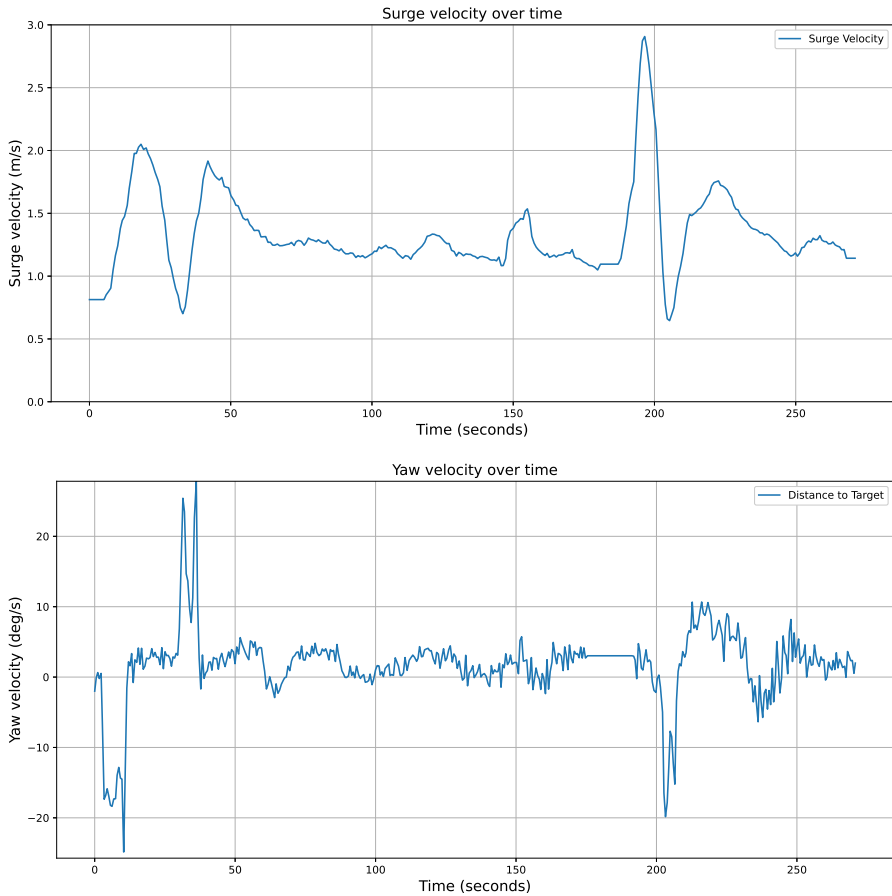


Figure 5.12: Circular line target tracking - Surge and yaw velocity - Pole placement gains

### Trial and Error Gains

Figure 5.13 shows the vessel having a very similar response to that of the simulator. After intercepting the target, the vessel quickly adjusted its heading and surge velocity to reach the target and closely follow it throughout the rest of the test.

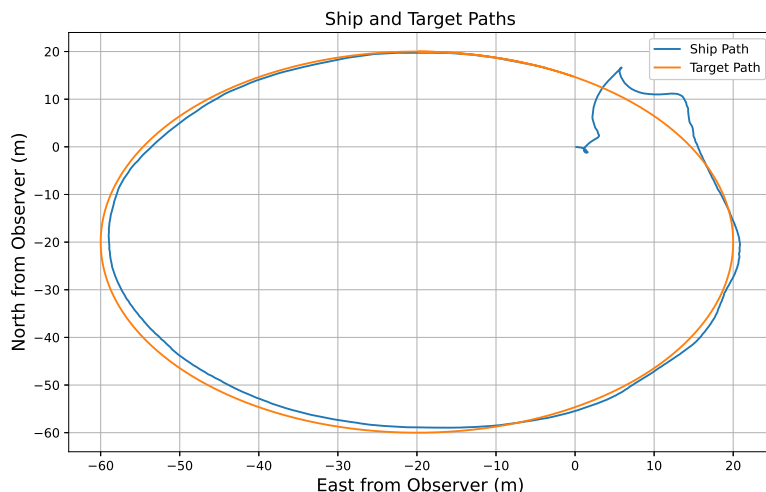


Figure 5.13: Circular target tracking - Target and vessel path - Trial and error gains

The corresponding control signals and velocities in Figures 5.14 and Figure 5.15 display the vessel with much more smooth and controlled movement. The vessel only took around 25 seconds to catch up to the target, slightly reducing its speed whenever it is about to pass the target position, and perfectly tracking it until the end of its deployment.

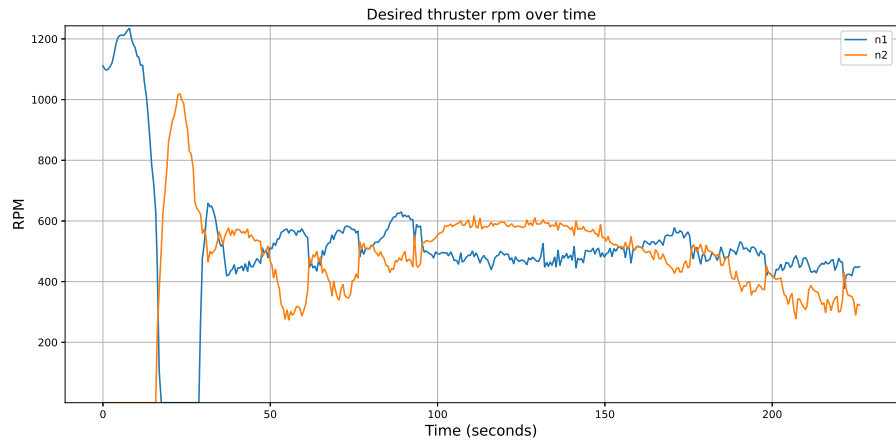


Figure 5.14: Circular line target tracking - Control signals - Trial and error gains

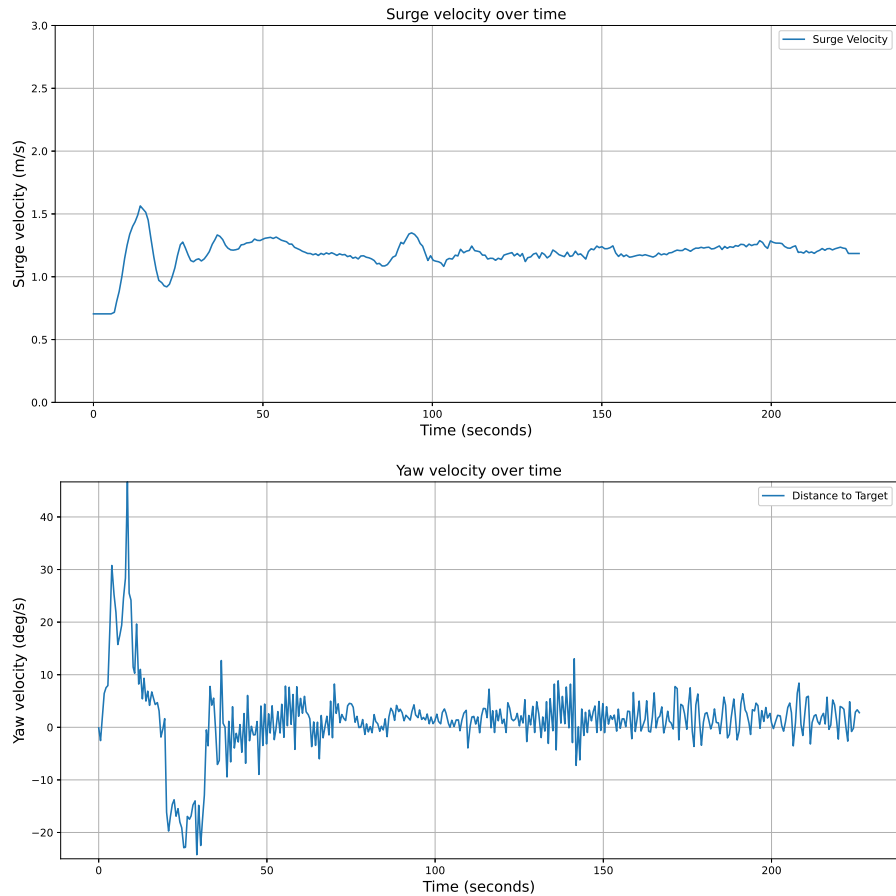


Figure 5.15: Circular line target tracking - Surge and yaw velocity - Trial and error gains

## 5.4 Summary of Results

Although differences from the simulated and physical results are apparent, these discrepancies are likely due to unmodeled damping forces and external factors such as wind and waves in the simulator. While the calculated gains produced better results in the simulations of both cases, the gains determined by trial and error yielded better results in the practical tests, highlighting a reality-gap in the simulator. This could be attributed to higher values in the heading controller with the practically determined gains, which might be better suited for quickly dealing with unpredictable forces acting on the vessel. However, values presenting promising outcomes in the simulator demonstrated effective real-world results, indicating that the simulator is a working tool for tuning the gains and other controller implementations before practical deployments.

Despite variations in the time to target and oscillations around the target path, all scenarios returned adequate results. In instances where the vessel deviated from the desired path, the time required again reach the target was mostly negligible. Ultimately, this underscores an optimization problem in identifying the optimal controller gains. The practically obtained values do however return promising results, with high proficiency in rapid and smooth heading adjustments, quickly reaching the target before following it in a controlled fashion in both the straight line and circular cases.

# Chapter 6

## Discussion

### Oscillations between target path

Time before reaching the target depends largely on the starting orientation of the USV. In the straight-line cases, it was discovered that where the starting position has small to no heading errors, it would quickly reach the target due to the smaller distances. However, it would overshoot and oscillate between the target path before perfectly tracking the target. In cases where the vessel's heading was initially orientated opposite to the target, the controller would first commit to heading adjustments, while the target would already be traveling. This ultimately resulted in the USV following a smoother path to intercept the target, slowing down sufficiently as the target was within the acceptable radius. In the controller gains, while the practically determined gains in the heading controller are higher in all three variables, the  $K_d$  value is more than ten times higher. This could counteract rapid changes in the early response of the controller, leading to reduced overshooting in cases where the vessel starting position is in close proximity to the target. It is possible that increasing the derivative portion of the pole placement gains would improve the system performance. Another potential solution to early path oscillations would be to increase the distance to the target radius where the integral limiter is activated in the surge controller. This could, however, negatively impact the vessel's ability to follow the target closely at higher velocities, where the trial-and-error values are currently able to follow a target velocity of up to  $2m/s$ . Most oscillations were found to be negligible in size, while completely dissipating in extended operation. The differences between linear PID controllers compared to prediction based ones such as NMPC were made apparent, where the ability to predict the target path could have improved on the target tracking in the initial stages of each test.

### Sensor Initialization Errors

Errors in the initial logged values happened repeatedly during the final tests, where these values had significant discrepancies between the actual system state in its position and velocity. While the cause of these errors is not certain, they could be created by a warm-up period in the sensor systems before they stabilize to provide accurate readings. If this is an initialization error in the GNSS, it could be caused by a time delay before the sensors acquire a satellite signal. The Kalman filter in the INS could also cause reading errors. As discussed in section 3.1, due to a Kalman filter being a prediction-based model it will require a set amount of readings before being able to produce reliable outputs. Additionally, the latency between the sensors and the shore station could result in the initial data being incomplete. A consequence of this

is in calculating the surge velocity based on the vessel's travel over time, where mistakes in the positional data could make it appear like the vessel travels much faster than the actual velocity.

Although these initial readings appear erratic, they do not impact the system's performance and will not require significant modifications. While some of the initial values are already discarded in each test, increasing the number of disposed readings would prevent errors. In cases where accurate readings of the first values are crucial, a warm-up period can also be initiated, setting the starting position further away or allowing the data collection to happen before the test is initialized. To ensure that the graphical representations were reflective of the actual system performance, any problematic values from the first rows of the CSV files were manually modified to match the following correct values. Additionally, to guarantee an accurate representation of the surge velocity, the average velocity was used in the plots, while interpolating for readings where the positional data would return to zero, removing inaccuracies.

### Control Bandwidth Approximation

As discussed in Fossen (2021, pp. 528–529) the control bandwidth ( $\omega_b$ ) is found by the first frequency where a control signal reaches -3dB ( $\approx 70.71\%$ ) of its maximum value when a step input is applied. This could be obtained by creating either a Python or MATLAB function that evaluates the frequency response and identifies at which point the magnitude of the response falls to the aforementioned percentages. A Bode plot could be utilized to visualize this, which would allow for accurately determining the frequency of this cutoff.

The control bandwidth used in the pole placement calculations is a rough estimate based on the physical response of the system. As the time constant, which is the time it takes to reach approximately 63.2% of the final value, is roughly inversely proportional to the control bandwidth, it can be used to approximate this value, where:

$$\omega_b \approx \frac{1}{T} \quad (6.1)$$

However, as discussed in section 4.4, the time constant when changing to reverse thrust is significantly higher, at around three seconds, leading to a lower control bandwidth, unless only the values related to changing speeds in already ongoing thrust are being considered. Due to this, the chosen  $\omega_b$  value was based on the physical response of the system, but it is likely notably lower than the actual control bandwidth of the system. This was however realized in later stages of the project, with time constraints preventing modeling for and testing with other values.

Another potential simplified solution would have been to calculate the weighted harmonic mean to still emphasise the lower time constant value by:

$$T = \frac{2}{\frac{1}{T_1} + \frac{1}{T_2}}, \quad \omega_b \approx \frac{1}{T} \approx 0.67 \text{ rad/s} \quad (6.2)$$

Where  $T_1$  displays the time constant in changing thrust in the current orientation, and  $T_2$  the time constant when changing thrust orientation. This would result in a higher control bandwidth, indicating a slightly higher efficiency in rapid heading adjustments. Another possibility is simply using the time constant  $T_1 = 1s$  where  $\omega_b \approx 1$  due to the vessel only chancing to negative thrust when there is a considerable heading error. However, a higher responsiveness could

lead to increased sensitivity to noise from wind and waves, as the controls are not designed to filter out such disturbances. Without additional testing it is difficult to conclude if this would have a large effect on the system performance, and whether using a higher bandwidth in the pole placement calculations would have led to improved performance.

### Test Inconsistencies

Inconsistencies in the testing procedures might have led to misleading results, making it difficult to compare the different tests. Where the practical tests in Figure 5.2 had the target start ten meters west of the vessel, the second straight line test in Figure 5.5 had the USVs starting position 80 meters away from the target. The close proximity in the initial test has the vessel reaching the target much earlier, reducing its ability to perform gradual heading adjustments during the first stages. Similarly in case 2, the initial test in Figure 5.10 has a starting position 40 meters south and 30 meters east, while the second test in Figure 5.13 commences 20 meters south-east. Although the scale is much smaller in the circular test it is difficult to conclude the physical effect of these inconsistencies.

This was ultimately a result of determining a path based on the current starting position of the shore station. By implementing a function translating this to be based on the current position and heading of the vessel, the required path in each test would be the same, improving the comparability of the results.

### Final Results

While the overall results of the practical deployment of the Otter USV controllers were positive, the discussed factors, such as determining the correct control bandwidth in conjunction with the testing procedure inaccuracies makes it difficult to conclude if the results would be different given similar starting conditions in all practical tests. Additionally, completing more tests under different wind and wave conditions would improve the understanding of how the vessel is able to operate under varying conditions. The results do however present a working control system for the Otter USV, available to use in future research at the Oceanlab OsloMet.

# Chapter 7

## Concluding remarks and further work

This thesis demonstrated the development and implementation of both PI surge and PID heading controllers to the Otter USV, with the objective of improving on these controllers by the use of a simulator, before practically deploying the vessel. Additionally, specialized clamps were designed and implemented for the use of an SBL acoustic receiver. This served as preliminary work towards research in underwater optical communication relays, where the USV can use sensor outputs to autonomously track targets by the assistance of the implemented controllers.

The thesis presented techniques in integrating control systems with sensor outputs, however did not practically test beyond simulated targets due to time constraints. Tests involved simulated scenarios and practical deployment with the vessel tracking virtual targets in the NED frame, where the USV successfully maintained the desired position within the target's radius. Where the tests compared controller gains determined through pole placement calculations and practical adjustments, a reality-gap between the simulations and the physical system response was seen. With inconsistencies in the testing procedures and too few practical tests, it was difficult to draw definitive conclusions on comparability of the system's performance in the different tests. Whereas the heading controller gains obtained through modeling the vessel as a mass-damper system saw inferior performance in comparison to the gains obtained through an empirical trial-and-error approach, this was likely due to a modeling error. However, the results indicate that the PI and PID controllers offer robust and reliable performance in both the simulated environment and in real-world deployment.

### 7.1 Further Work

Future work should consider the modeling of the vessel, improving on the pole placement calculations by finding the correct control bandwidth to discover the optimal gains for the controllers. Additionally, albeit negligible, the reality-gap between the practical tests and the simulations could be improved on by adding damping effects to the simulator. Completing new tests with a more standardized testing procedure would also provide more reflective results of the actual performance than what was documented in this thesis.

The implementation of the UGPS was suboptimal and should work seamlessly with the rest of the Otter API, where the system should communicate data wirelessly to a shore station. The Python program for the Water Linked UGPS G2 should also be implemented in the API

for the Otter. Wireless communication can be done with socket communication, where the shore station is able to log the locations in a CSV file for later plotting, similar to the system currently implemented for the Otter USV's positional data.

As the SBL antenna was rotated to prevent the nodes from getting in the way of the optical modem, the antenna's coordinate system was equally rotated. Therefore, the coordinate system should be transformed in the program to the correct direction to match the body-frame  $\{b\}$  of the USV.

In future research endeavors into UOWC, the bracket system should be enhanced to better withstand hydrodynamic damping effects. Additionally, a socket communication system between the sensor and the shore station must be established and integrated with the Otter API.

# Bibliography

- Akdağ, M., Fossen, T. I., & Johansen, T. A. (2022). Collaborative collision avoidance for autonomous ships using informed scenario-based model predictive control. *IFAC-PapersOnLine*, 55(31), 249–256.
- Alcocer, A., Oliveira, P., & Pascoal, A. (2006). Underwater acoustic positioning systems based on buoys with gps. *Proceedings of the Eighth European Conference on Underwater Acoustics*, 8, 1–8.
- Alkan, R. M., Erol, S., İlçi, V., & Ozulu, İ. M. (2020). Comparative analysis of real-time kinematic and ppp techniques in dynamic environment. *Measurement*, 163, 107995.
- Ang, K. H., Chong, G., & Li, Y. (2005). Pid control system analysis, design, and technology. *IEEE transactions on control systems technology*, 13(4), 559–576.
- Asada, T., Inoue, K., & Onogi, S. (1976). Diffusion in the nylon 12 and water system. *Polymer Journal*, 8(1), 21–29.
- Azzeri, M., Adnan, F., & Zain, M. M. (2015). Review of course keeping control system for unmanned surface vehicle. *Jurnal Teknologi*, 74(5), 11–20.
- Balestrieri, E., Daponte, P., De Vito, L., & Lamonaca, F. (2021). Sensors and measurements for unmanned systems: An overview. *Sensors*, 21(4), 1518.
- Breivik, M., Hovstein, V. E., & Fossen, T. I. (2008). Straight-line target tracking for unmanned surface vehicles.
- Caccia, M., Bibuli, M., Bono, R., & Bruzzone, G. (2008). Basic navigation, guidance and control of an unmanned surface vehicle. *Autonomous Robots*, 25(4), 349–365.
- Cao, N., Lu, S., Yao, R., Liu, C., Xiong, Q., Qin, W., & Wu, X. (2020). A self-regenerating air-laid paper wrapped asa 3d cone-shaped janus evaporator for efficient and stable solar desalination. *Chemical Engineering Journal*, 397, 125522.
- Cisco Systems. (2024). *What is 802.11ac?* Retrieved May 11, 2024, from <https://www.cisco.com/c/en/us/products/wireless/what-is-802-11ac.html#~q-a>
- Denys, P., Liggett, A., Odolinski, R., Pearson, C., Stewart, D., & Winefield, R. (2017). Networkrtk-new zealand.
- Fossen, T. I. (2021). *Handbook of marine craft hydrodynamics and motion control*. John Wiley & Sons.
- Fossen, T. I. (2023). *Python vehicle simulator*. Retrieved December 18, 2023, from <https://github.com/cybergalactic/PythonVehicleSimulator>
- Fossen, T. I. (1991). *Nonlinear modelling and control of underwater vehicles*. Universitetet i Trondheim (Norway).
- Frafjord, A. J. (2023). *Target tracking control for an unmanned surface vessel: Optimal control vs reinforcement learning* [Master's thesis, OsloMet-storbyuniversitetet].
- Google Earth. (2024a). *Fillipstad veien 7, 0252 oslo, 59°54'26"n 10°43'05"e*. Retrieved April 22, 2024, from <https://earth.google.com/web/@59.90840046,10.71980268,-0.51925767a,481.56376321d,35y,105.47498616h,46.86304516t,0r/data=MikKJwolCiExZTJUdnP SQ1BuRGU3SDgyT>

- Google Earth. (2024b). *Oslofjord, 59°52'53"n 10°44'25"e*. Retrieved April 22, 2024, from <https://earth.google.com/web/@59.88157734,10.74028536,-0.19545697a,1000d,30y,0h,0t,0r/data=MikKJwolCiExaEtnRVZGdER1MUc3NWppNTJwcnNxRFVKaFBiFFTOWkgAToDCgEw>
- Graziano, A., Teixeira, A., & Soares, C. G. (2016). Classification of human errors in grounding and collision accidents using the tracer taxonomy. *Safety science*, 86, 245–257.
- Gresberg, S. A. S., Johnsen, L. S., & Stensrud, S. (2023, November). *Application programming interface for an autonomous surface vessel* [Assignment submitted for ELVE3610 - Introduction to robotics, OsloMet]. [https://github.com/SigurdGresbe/Otter\\_Thesis/blob/main/ELVE3160\\_report.pdf](https://github.com/SigurdGresbe/Otter_Thesis/blob/main/ELVE3160_report.pdf)
- Kafle, A., Luis, E., Silwal, R., Pan, H. M., Shrestha, P. L., & Bastola, A. K. (2021). 3d/4d printing of polymers: Fused deposition modelling (fdm), selective laser sintering (sls), and stereolithography (sla). *Polymers*, 13(18), 3101.
- Kaushal, H., & Kaddoum, G. (2016). Underwater optical wireless communication. *IEEE access*, 4, 1518–1547.
- Khodarahmi, M., & Maihami, V. (2023). A review on kalman filter models. *Archives of Computational Methods in Engineering*, 30(1), 727–747.
- Kim, D., Hirayama, K., & Okimoto, M. (2015). Ship collision avoidance by distributed tabu search. *TransNav: International Journal on Marine Navigation and Safety of Sea Transportation*, 9(1).
- Kjelsaas, M. (2022). *Making an ai powered asv* [Master's thesis, OsloMet-storbyuniversitetet].
- Kretschmann, L., Burmeister, H.-C., & Jahn, C. (2017). Analyzing the economic benefit of unmanned autonomous ships: An exploratory cost-comparison between an autonomous and a conventional bulk carrier. *Research in transportation business & management*, 25, 76–86.
- Li, W., Ge, Y., Guan, Z., Gao, H., & Feng, H. (2023). Nmpc-based uav-usv cooperative tracking and landing. *Journal of the Franklin Institute*, 360(11), 7481–7500.
- Lien Wennersberg, L. A. (2023). Gjenombrudd for autonome skip. *SINTEF*. Retrieved January 10, 2024, from <https://www.aftenposten.no/norge/i/4ovG3o/ap-sp-hoeyre-frp-og-krf-sikrer-flertall-naa-kan-e-tjenesten-starte-masseovervaaking-i-norge>
- Liu, Z., Zhang, Y., Yu, X., & Yuan, C. (2016). Unmanned surface vehicles: An overview of developments and challenges. *Annual Reviews in Control*, 41, 71–93.
- Maritime Robotics. (2020). *Otter usv user manual* [Rev. 1.4]. <https://www.maritimerobotics.com/otter>
- Maritime Robotics. (2024). *Otter unmanned surface vehicle*. Retrieved January 2, 2024, from <https://www.maritimerobotics.com/otter>
- MarkForged, Inc. (2024). Composites material datasheet [Accessed: 2024-05-21]. <https://s3.amazonaws.com/mf.product.doc.images/Datasheets/Material+Datasheets/CompositesMaterialDatasheet.pdf>
- Martin, C. C., Winters, J. H., & Sollenberger, N. R. (2000). Multiple-input multiple-output (mimo) radio channel measurements. *Vehicular Technology Conference Fall 2000. IEEE VTS Fall VTC2000. 52nd Vehicular Technology Conference (Cat. No. 00CH37152)*, 2, 774–779.
- Martinsen, A. B., Lekkas, A. M., & Gros, S. (2019). Autonomous docking using direct optimal control. *IFAC-PapersOnLine*, 52(21), 97–102.
- Melenka, G. W., Cheung, B. K., Schofield, J. S., Dawson, M. R., & Carey, J. P. (2016). Evaluation and prediction of the tensile properties of continuous fiber-reinforced 3d printed structures. *Composite Structures*, 153, 866–875.

- Montalvão, G., Moshrefi-Torbat, M., Hamilton, A., Machado, R., & João, A. (2020). Behaviour of 3d printed pla and pla-pha in marine environments. *IOP Conference Series: Earth and Environmental Science*, 424(1), 012013.
- Nise, N. S. (2011). *Control systems engineering* (Sixth). John Wiley & Sons, Incorporated.
- Penas, A. A. (2009). Positioning and navigation systems for robotic underwater vehicles. *Doctor thesis, Instituto Superior Tcnico*.
- Pocwiardowski, P. (2023). Essential resource management in dredging hydrographic surveying using usv and sv. *2023 IEEE Underwater Technology (UT)*, 1–4.
- Saksvik, I. B., Alcocer, A., Hassani, V., & Pascoal, A. (2022). Target tracking of an underwater glider using a small unmanned surface vessel. *IFAC-PapersOnLine*, 55(31), 478–483.
- SBG Systems. (2023). *Ellipse series miniature high performance inertial sensors* [Rev. 2.4]. [https://www.sbg-systems.com/wp-content/uploads/Ellipse\\_Series\\_Leaflet.pdf](https://www.sbg-systems.com/wp-content/uploads/Ellipse_Series_Leaflet.pdf)
- Schirripa Spagnolo, G., Cozzella, L., & Leccese, F. (2020). Underwater optical wireless communications: Overview. *Sensors*, 20(8), 2261.
- SNAME, T. (1950). Nomenclature for treating the motion of a submerged body through a fluid. *The Society of Naval Architects and Marine Engineers, Technical and Research Bulletin*, (1950), 1–5.
- Stateczny, A., Specht, C., Specht, M., Brčić, D., Jugović, A., Widżgowski, S., Wiśniewska, M., & Lewicka, O. (2021). Study on the positioning accuracy of gnss/ins systems supported by dgps and rtk receivers for hydrographic surveys. *Energies*, 14(21), 7413.
- Techet, A. H. (2005). Added mass. Retrieved March 17, 2024, from <https://web.mit.edu/2.016/www/handouts/2005Reading6.pdf>
- Verfuss, U. K., Aniceto, A. S., Harris, D. V., Gillespie, D., Fielding, S., Jiménez, G., Johnston, P., Sinclair, R. R., Sivertsen, A., Solbø, S. A., et al. (2019). A review of unmanned vehicles for the detection and monitoring of marine fauna. *Marine pollution bulletin*, 140, 17–29.
- Wan, L., Zeng, J., Li, Y., Qin, H., Zhang, L., & Wang, J. (2019). Neural observer-based path following control for underactuated unmanned surface vessels with input saturation and time-varying disturbance. *International Journal of Advanced Robotic Systems*, 16(5), 1729881419878071.
- Wang, Q., Cui, X., Li, Y., & Ye, F. (2017). Performance enhancement of a usv ins/cns/dvl integration navigation system based on an adaptive information sharing factor federated filter. *Sensors*, 17(2), 1–5.
- Water Linked AS. (2017). Water linked underwater gps api examples [Accessed: 2024-05-16].
- Water Linked AS. (n.d.-a). Robust positioning system - underwater gps g2 [Accessed: 10-May-2024, publication date not available]. <https://waterlinked.com/web/content/7539?unique=0e0957583b670554b27abb667a70927bcf35c6a7>
- Water Linked AS. (n.d.-b). Underwater gps quickstart guide [Accessed: 2024-05-13, publication date not available]. <https://waterlinked.github.io/underwater-gps/quickstart/>
- Water Linked AS. (n.d.-c). Waterlinked - u1 locator [Accessed: 2024-05-13, publication date not available]. <https://waterlinked.com/shop/underwater-gps-g2-locator-u1-122#attr=ZeroTier>.
- Zerotier. (2024). *Zerotier vpn*. Retrieved March 5, 2024, from <https://www.zerotier.com/>
- Zhang, C., Cheng, P., Lin, B., Zhang, W., & Xie, W. (2023). Drl-based target interception strategy design for an underactuated usv without obstacle collision. *Ocean Engineering*, 280, 114443.
- Zhao, Y., Ma, Y., & Hu, S. (2021). Usv formation and path-following control via deep reinforcement learning with random braking. *IEEE Transactions on Neural Networks and Learning Systems*, 32(12), 5468–5478.

# **Appendix A**

## **GitHub Repository**

Thesis GitHub Repository: [https://github.com/SigurdGresbe/Otter\\_Thesis](https://github.com/SigurdGresbe/Otter_Thesis). All code produced through this project is found in this repository, ran on the specifications described in Appendix B.

# Appendix B

## Software and Hardware

Software	Version
Windows	11
Python	3.10
Pymap3D	3.0.1
Pandas	2.2.2
Numpy	1.23.1
Scipy	1.9.1
Matplotlib	3.5.2

Table B.1: Software list

All simulations and live runs were performed on a Komplett Khameleon P9 pro laptop with the hardware components:

Hardware	Type
CPU	9th Gen Intel(R) Core(TM) i7-9750H 2.60 GHz
GPU	RTX 2070 MaxQ Laptop
RAM	32 GB DDR4

Table B.2: Hardware list

# Appendix C

## Otter USV Physical Parameters

Table C.1: Physical parameters of Otter USV from Maritime Robotics (2020) and Fossen (2023)

Parameter	Description	Value	Unit
$m$	Vessel Mass	62.0	[kg]
$L$	Vessel Length	2.0	[m]
$B$	Vessel Width (Beam)	1.08	[m]
$r_g$	Hull center of gravity	$[0.2, 0, -0.2]^\top$	[m]
$R_{66}$	Radii of gyration (Yaw)	$0.25 \cdot L$	[m]
$T$	Time constant (Vessel already in motion)	1.0	[s]
$u_{max}$	Maximum velocity	3.08	[m/s]
$X_u$	Linear damping in surge	-77.55	[ $\cdot$ ]
$Y_v$	Linear damping in sway	0	[ $\cdot$ ]
$N_r$	Angular damping in yaw	-51.03	[ $\cdot$ ]
$I_z$	Inertia around the z-axis	15.5	[kg·m <sup>2</sup> ]

# Appendix D

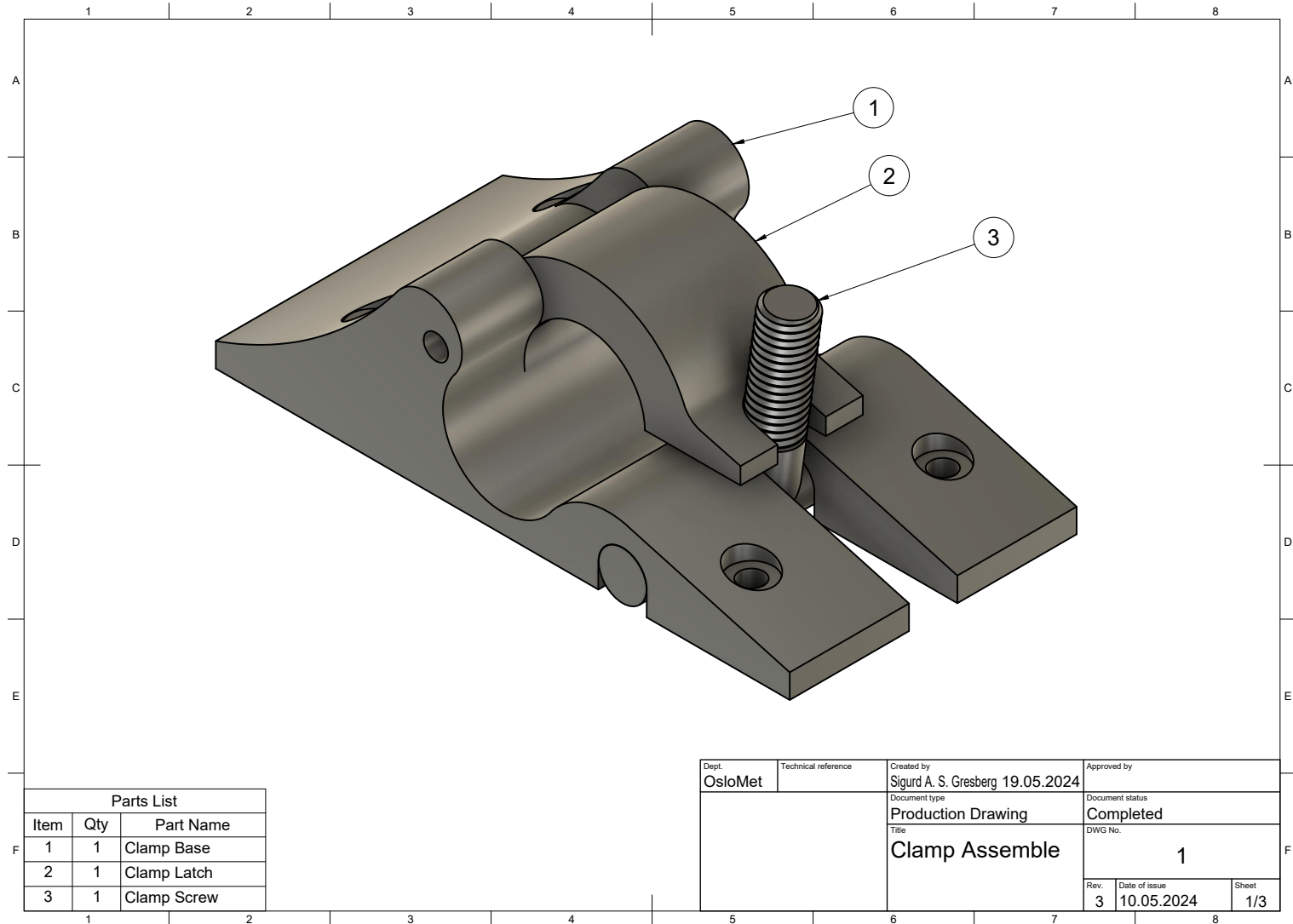
## Contribution Table

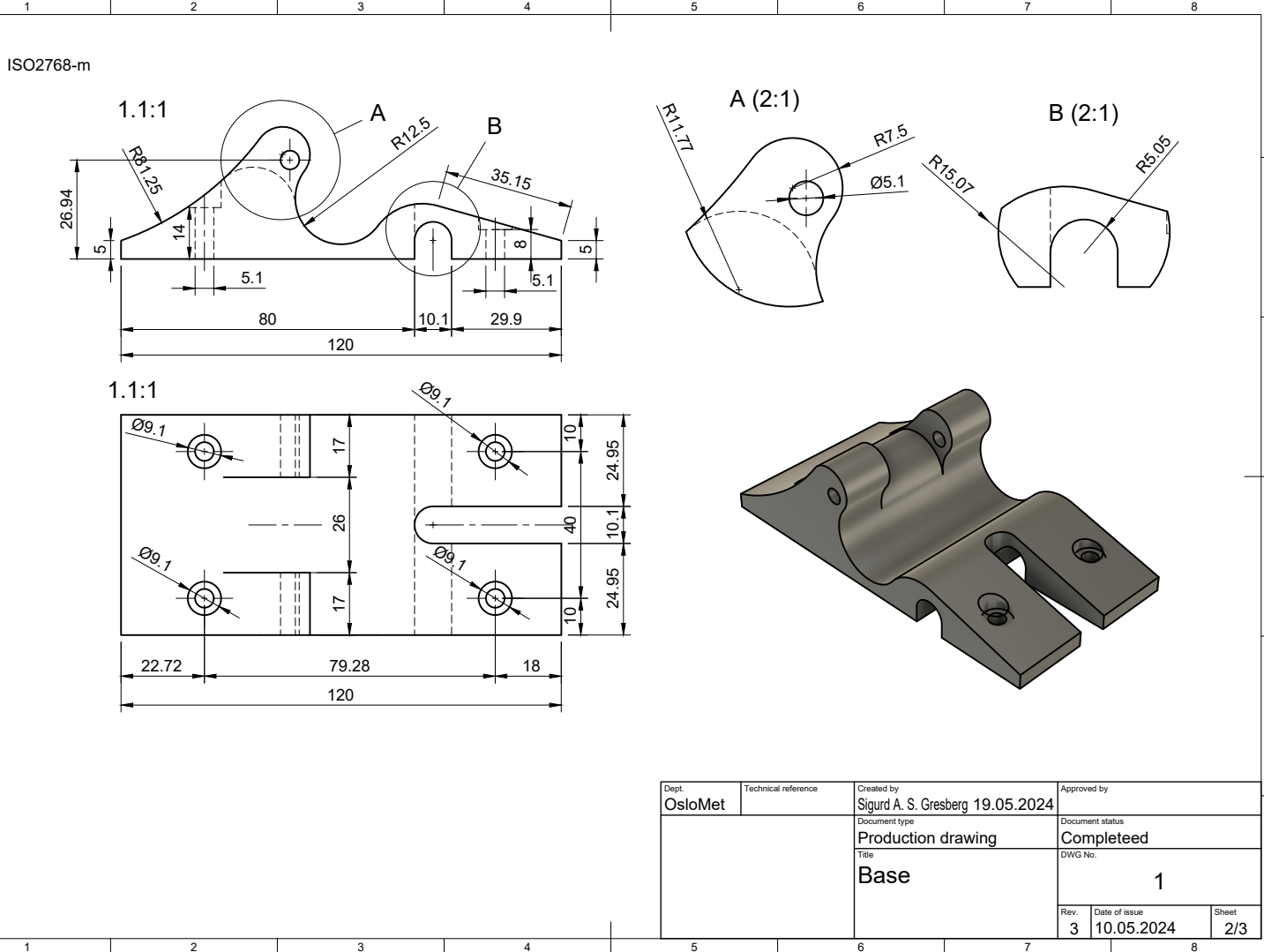
Student	Written contribution	Technical contribution
Sivert	Total 30%	40% - code, simulator and live guidance development.
Lars	Total 40%	25% - code, API, testing and modeling.
Sigurd	Total 30%	35% - code API, mechanical design of brackets,.

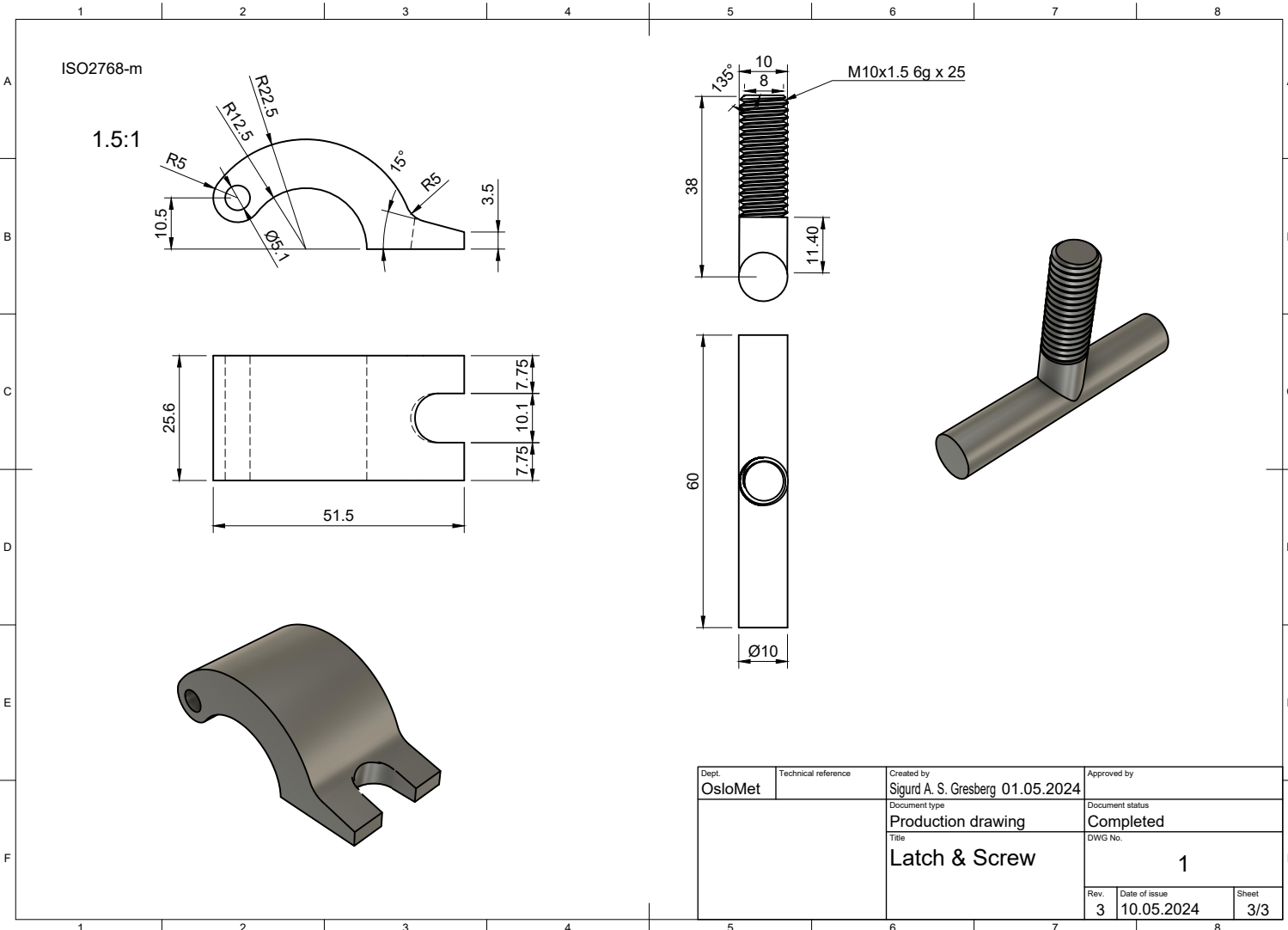
Several key parts of the document and code were worked on in conjunction with other group members, thus an attempt was made to estimate a percentage contribution to the entire project.

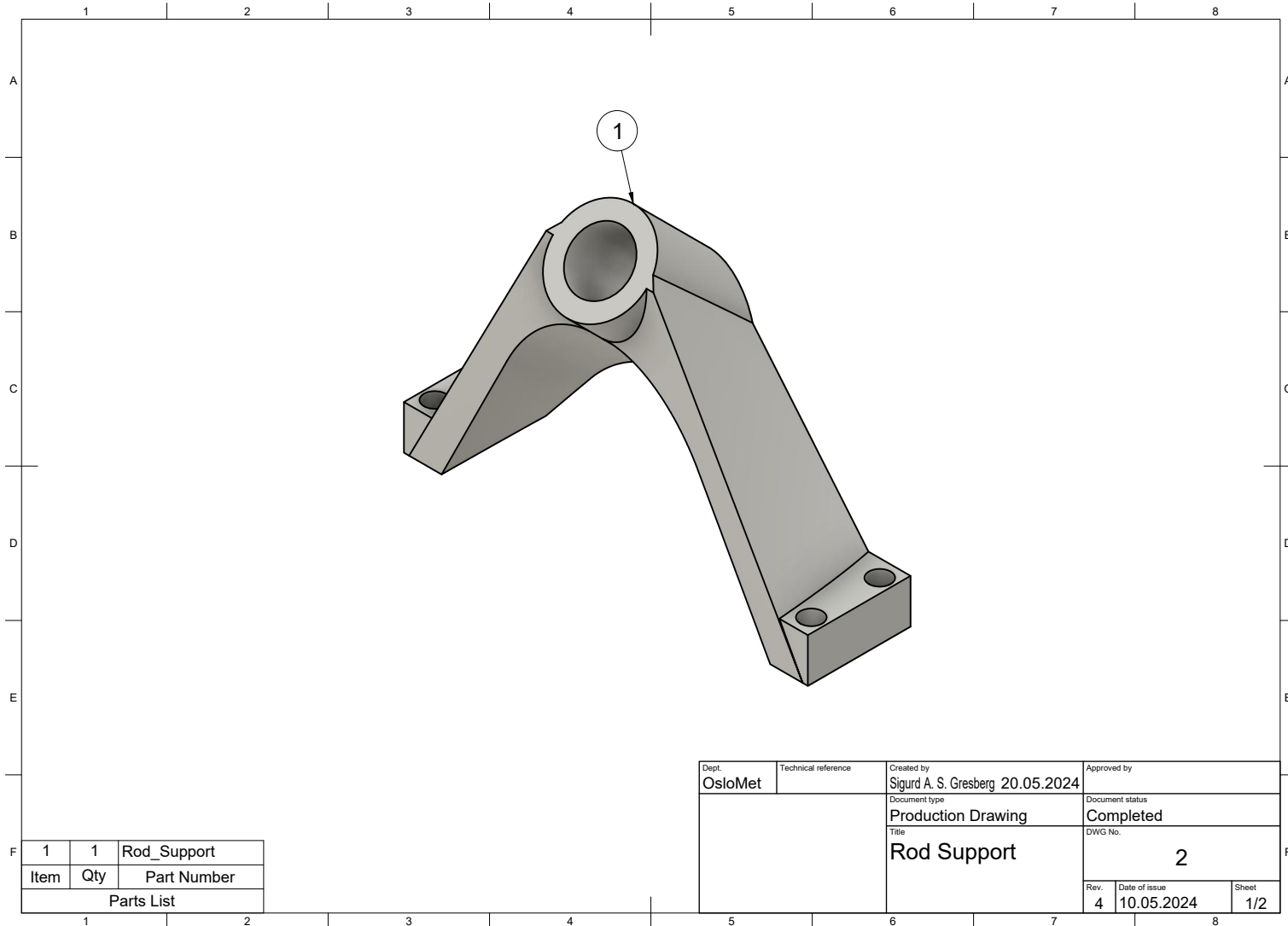
# **Appendix E**

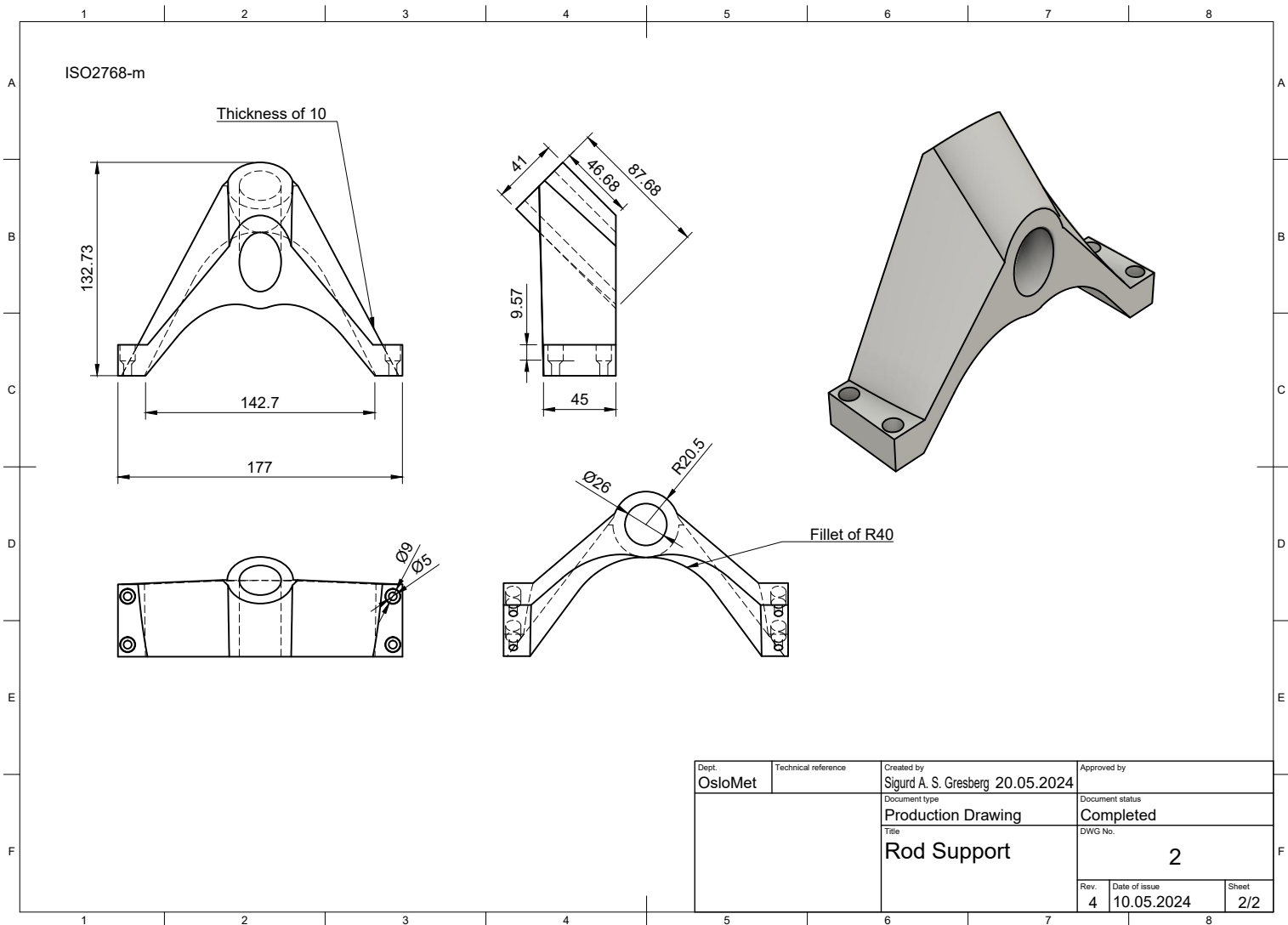
## **Technical drawings**







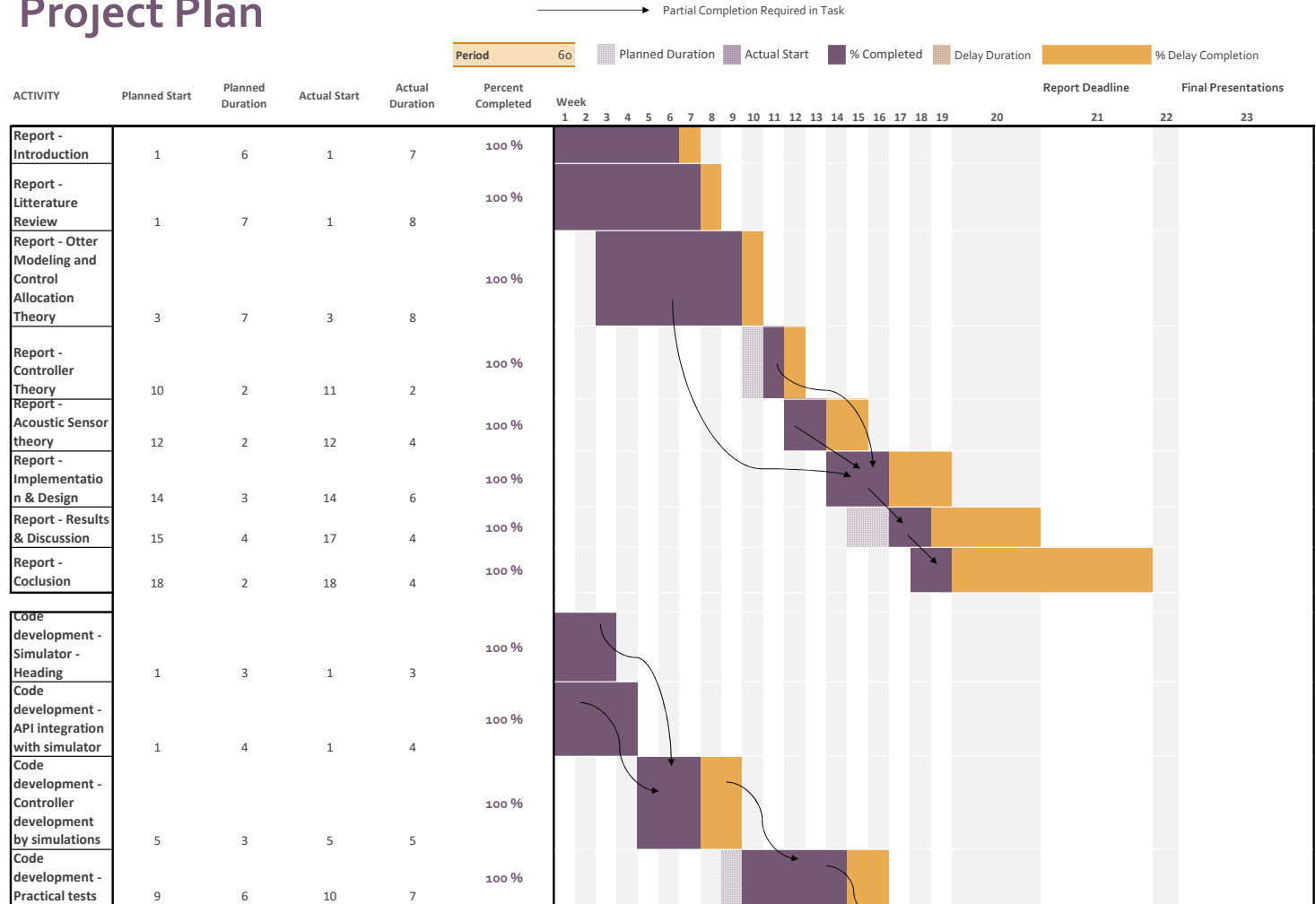




# **Appendix F**

## **Gannt Diagram**

# Project Plan





## **Appendix G**

### **Functional Specification**

# Functional Specification Document

**Title:** Target Tracking for Unmanned Surface Vehicles

**Date:** May 23, 2024

**Authors:** Sigurd Aleksander Salomonsen Gresberg, Lars Skogen Johnsen, Sivert Stensrud

**Institution:** Oslo Metropolitan University - OsloMet

**Faculty:** Faculty of Technology, Art, and Design

**Department:** Institute of Mechanical, Electrical, and Chemical Engineering

## 1. Introduction

The purpose of this document is to define the functional requirements for the implementation of controllers and an acoustic sensor for the Otter Unmanned Surface Vessel (USV) to facilitate future work on Underwater Optical Wireless Communication (UOWC) sensors. The main goal is to develop and implement Proportional-Integral-Derivative (PID) and Proportional-Integral (PI) controllers for target tracking operations.

## 2. System Overview

The system involves the Otter USV equipped with:

- PID and PI controllers.
- SBL acoustic sensors.
- Underwater Optical Wireless sensors.

The focus is on enhancing the Otter USV's ability to perform accurate target tracking using both simulated and real-world experiments.

## 3. Functional Requirements

### 3.1 Controller Implementation

**Objective:** Implement PID and PI controllers for regulating the heading and velocity of the Otter USV.

- **PID Controller:** Used for heading control.

- Proportional gain ( $K_p$ )
- Integral gain ( $K_i$ )

- Derivative gain ( $K_d$ )
- **PI Controller:** Used for surge (velocity) control.
  - Proportional gain ( $K_p$ )
  - Integral gain ( $K_i$ )

### Tuning Methods:

- Pole placement.
- Heuristic trial-and-error.

### 3.2 Controller Functions

#### Control Allocation:

- Compute required thrust for both heading and velocity.
- Limit total force to ensure system stability.

#### Throttle Map:

- Convert control signals to desired RPM values.
- Linearize control signal outputs to improve stability.

#### Integral Cap and Reset:

- Cap the integral component to prevent overshooting.
- Reset integral component upon reaching the target to ensure stability.

#### Error Handling:

- Handle initial sensor errors by discarding erroneous readings.

### 3.3 Sensor Integration

#### UGPS G2 Acoustic Sensor:

- Attach modem securely to the Otter USV.
- Implement Python program for data acquisition.

- Log data to CSV for post-processing and visualization.
- Communicate sensor data wirelessly to the shore station.

#### **Optical Modem:**

- Attach modem securely to the Otter USV.
- Ensure system compatibility for future UOWC research.

#### **3.4 Testing Procedures**

##### **Simulated Testing:**

- Simulate target tracking in both straight-line and circular paths.
- Compare performance of controllers with pole placement and deterministic tuning methods.

##### **Practical Testing:**

- Conduct tests in sheltered and open water conditions.
- Evaluate the impact of real-world factors such as wind and waves.
- Standardize starting conditions to ensure consistent results.

#### **3.5 Data Handling**

- Log positional and sensor data to CSV files.
- Ensure data integrity by filtering out initialization errors.
- Use averaged values for velocity to enhance accuracy in plots.

### **4. Non-Functional Requirements**

##### **Performance:**

- Ensure the USV tracks targets with minimal oscillation and overshoot.
- Optimize controller response time for real-world conditions.

##### **Reliability:**

- Implement error handling for sensor initialization.
- Ensure continuous communication with the shore station.

### **Usability:**

- Develop a user-friendly API for the Otter USV.

### **5. Future Work**

- Improve hydrodynamic modeling of the Otter USV.
- Enhance the acoustic localization integration.
- Conduct practical tests under varying environmental conditions.
- Develop communication protocols for real-time data transmission to shore stations for the acoustic sensor.